Sunniva Omdal

Competitive CO2 capture using montmorillonite clay minerals

Role of pressure and interlayer cations

Master's thesis in Applied physics and mathematics
Supervisor: Jon Otto Fossum

June 2023

NTNU
Norwegian University of
Science and Technology

Sunniva Omdal

Competitive CO2 capture using montmorillonite clay minerals

Role of pressure and interlayer cations

Master's thesis in Applied physics and mathematics
Supervisor: Jon Otto Fossum
June 2023

Norwegian University of Science and Technology
Faculty of Natural Sciences
Department of Physics

NTNU
Norwegian University of
Science and Technology

1 Preface

This thesis concludes my master thesis in applied physics on the swelling of natural montmorillonites in the presence of carbon dioxide. The experiments have been carried out in the fall semester of 2022 and the spring semester of 2023 in the third floor of Realfagbygget at the Laboratory of Soft and Complex Matter Studies at NTNU in Trondheim, the European Synchotron Radiation Facility in Grenoble, France and at the Institute for Material Technology at NTNU in Trondheim. All experiments were done for the Soft and Complex Matter group. Most of the ESRF experiments were carried out as part of my specialization project in the fall, which have worked as a basis to this thesis.

I would like to thank my supervisor Jon Otto Fossum for providing me with unique opportunities this past year. I am also grateful for all the help I got from Konstanse K. Seljelid, who has acted as my co-supervisor. I would also like to thank my study colleagues and friends who have contributed to a pleasant study period. My gratitude goes also to my family, who is always there for me, and particularly my father for helping me perfection this thesis. Without any of you, I would not be where I am today.

Abstract

The continuous increase of released greenhouse gases, in particular carbon dioxide, to the atmosphere has a harmful impact on the environment. In addition to emission reduction, it is necessary to establish effective ways of capturing these gases. It has previously been proved that certain clay minerals are competitive to other relevant porous materials for carbon capture. In recent work, combined experimental results from powder x-ray diffraction, Raman spectroscopy, and inelastic neutron scattering supported by density functional theory calculations studied on synthetic clay minerals were used to look at the carbon dioxide adsorption mechanisms in a pure defect free system. For future experiments, natural clays will be investigated in the context of this new mechanism, with the purpose of establishing the base for industrial carbon capture applications. In this thesis, natural bentonite and montmorillonite clay minerals are cation exchanged with nickel and iron. The montmorillonites have a similar crystal structure and are cheaper than the synthetic fluorohectorites. The aim is to map which of the natural clay minerals take up carbon dioxide, and how the different cations enhance this mechanism. Nickel fluorohectorites and iron fluorohectorites have previously proved to swell when exposed to carbon dioxide. The swelling in clays are determined from x-ray scattering experiments, where the lattice spacing in clay minerals are determined, and the lattice spacing disorder discussed. In addition, thermogravimetric analysis measurements are useful to determine how dry a clay mineral can be when the sample temperature is above 200°C. The montmorillonites nickel Crook1 and 2 are the most promising natural clays to take up carbon dioxide, while nickel bentonite does not take up carbon dioxide at all.

Samandrag

Det at utsleppa av drivhussgassa, og særleg karbon dioksid, i atmosfæren fortset å auke har ein sårande innverknad på miljøet. I tillegg til å redusere utslepp er det naudsynt å finne metodar for å fange desse gassane. Det har tidlegare vorte observert at nokre leire mineraler er konkurransedyktige som materiale for karbonfagst. Resultat frå tidlegare målingar med røntgendiffraksjon, Ramanspektroskopi, uealastisk nøytronspreiing og utrekningar med tettleiksfunksjonell teori av syntetisk leire viser at dei tek opp karbon dioksid. Vi ønsker å studere denne mekansimen i naturleg leire, med hensikt om å skape ein basis til industriell karbonfangst. I denne oppgavå vert naturlege bentonitt og montmorillonitt leirprøvar studert, både som dei er og etter å ha vorte kationutbytta med nikkel og jern. Montmorillonittane har ein liknande krystallstruktur, men er billegare, samanlikna med dei syntetiske fluorohektorittane. Målet er å kartlegge kva for nokre leirmineraler som er dei beste kandidatane til å fange karbon dioksid. Nikkel fluorohektorittane har tidlegare vist at dei utvidar seg når dei vert utsett for trykk frå karbon dioksid gass. Utvidelsen av leirelaga vert berekna ved hjelp av røntgenmålingar som måler korleis gitteravstanden og uordenen av den endrar seg med omsyn på trykk og temperatur. Det vert også utført termogravimetrisk analyse på prøvane for å bestemme kor tørr kvar leireprøve er, når temperaturen er over 200°C. Det visar seg at Montmorilloniten nikkel Crook1 og 2 har dei beste forutsetningane til å ta opp karbon dioksid, samtidig som nikkel bentonitt ikkje tek opp CO_2 i det heile teke.

Contents

List of Tables

List of Figures

2   Abbreviatons

CEC   cation exchange capacity

CO_2 Carbon dioxide

ESRF   European synchotron radiation facility

Fe   Iron

FTIR   Fourier-transform infrared spectroscopy

MNT   Montmorillonite

Ni   Nickel

NTNU   Norwegian University of Science and Technology

PXRD   Powder x-ray diffraction

TGA   Thermogravimetric analysis

WL   Water layer

XRD   X-ray diffraction

3 Introduction

The increased concentration of greenhouse gases in the atmosphere has doubled since the end of the Industrial Revolution and to this day. The continuous increase of released anthropogenic CO_2 gas disturbs the carbon cycle. Carbon dioxide is a vital gas for life on Earth, but the increased concentration has raised global concerns. The greenhouse gases trap thermal energy within the atmosphere, which lead to positive radiative forcing. Radiative forcing describes the net change in the radiation balance, where incoming UV radiation from the Sun and outgoing infrared radiation from the Earth are counted for. The ozone layer is the part of the atmosphere that limits the flux of short wave radiation to reach Earth's surface. The interaction of greenhouse gases with ozone destroys this layer, and increases the incoming radiation flux. This causes the average surface temperature on Earth to increase drastically, putting life as we know it at risk. With the increased concentration of atmospheric carbon dioxide, increases the amount of CO_2 in the oceans. As a consequence will the oceans become more acidic, and therefore also a more hostile environment for ocean living organisms. It is therefore important to reduce our carbon emissions. However, due to the current huge concentration of carbon dioxide in the atmosphere, the removal of the excess atmospheric carbon dioxide can not only be done by reducing our emissions. Solutions to capture and store this gas is of great interest as an approach to limit the climate changes upon us. Many are studying different materials suitable for carbon capture[12]. Emptied oil reservoirs as storage sites for the captured carbon dioxide have already been widely accepted as a potential solution. Therefore clay minerals, which are naturally abundant at such geological sites, are an expedient choice to study their adsorption mechanism of carbon dioxide.

Clay minerals are potential candidates because of their ability to hold high concentration of water molecules at certain temperatures and pressures compared to their own weight. The intercalation of the polar water molecule occurs in the interlayer where the oxygen atoms in water form temporary dipoles with cations in the clay. Despite the fact that CO_2 are non-polar molecules, recent findings show that they too can be adsorbed in certain clay minerals. The main conditions seem to be that they have a layer spacing above 10 Å for high pressure and low temperature levels, and that there is no water in the interlayer. Understanding how the mechanism work is of great interest, in order to take benefit of it as an industrial application. Clay minerals are cheaper and more environmental friendly compared to other suitable materials, like metal-organic frameworks. The clays that prove to adsorb CO_2, are an expedient choice to use for capturing carbon. Other findings show that the adsorption capacity in synthetic fluorohectorite clays increases as the layer charge is reduced. Exchanging nickel or iron cations in fluorohectorites gave the most efficient CO_2 adsorbing clays with an increase of layer spacing by 1 Å when exposed to 50 bar of CO_2[6]. A previous study on Sodium Montmorillonite SWy-2 show that the clay layers expand from 10.3 Å to 11.3 Å at room temperature when it was exposed to CO_2 in a pressure range between 1 and 50 bar[4]. Therefore, it is expected for montmorillonites exchanged with higher charge cations to adsorb CO_2 even better, which should be illustrated with a higher increase in basal distance. The CO_2 experiments on the natural clays which are discussed in this thesis, will be done at 27°C after they have been completely dried at 150°C, as long as the d-spacing is above 10 Å. The aim of the experiments is to determine which nickel cation exchanged natural clay minerals swell in response to CO_2. This will in turn give us an indication for which clay minerals take up CO_2. These clays will be studied further, using other measurement techniques to obtain a deeper understanding of the carbon dioxide reaction in the chosen clay minerals.

The cheaper and more environmental friendly clay minerals are the ones that are natural abundant, like montmorillonites, which are substituted with fluorohectorites in similar CO_2 experiments. The fluorohectorite clays are artificial synthesized smectites prepared at the univeristy of Bayreuth, Germany in supervision of Josef Breu, while montmorillonite clays are natural abundant smectites found in soils. The montmorillonites Crook1, Crook2 and Gonzales, bentonite and hydrobentonite all come from different reservoirs in the United States. Nickel Gonzales and nickel bentonite are considered to be the best montmorillonites for carbon capturing because of their high d-spacing when they are wet.

Previous XRD and FTIR experiments on natural kaolinite clay show that other types of natural clay minerals adsorb CO_2[1]. Smectites are the clay minerals known to swell the most in response to water intercalation. Montmorillonites are the natural smectites with the highest cation exchange capacity, and are exchanged with nickel cations, some are exchanged with iron cations, while other powders remain with their natural sodium or calcium cations for comparison. The cation exchange is applied in order to study how different cations influence the structural change in natural clays under the reaction with

carbon dioxide and water. The exchanged cations in montmorillonites are chosen according to which show to enhance the adsorption of carbon dioxide in fluorohectorites the most. Analyzing the change of the basal spacing in montmorillonites in response to temperature and pressure is a good first step to improve our understanding on how clays adsorb CO_2. Therefore comparing the degree of layer spacing increase in response to carbon dioxide is a good method to distinguish the preferred natural smectite and exchangeable cation.

The basal distance in different clay minerals are determined using wide angle x-ray scattering experiments. The x-ray data are collected from the Swiss-Norwegian Beamline(SNBL) 01 at ESRF in Grenoble. In the experimental setup, the temperature and pressure are controlled while continuously measuring the clay. The sample temperature is regulated by a Cryostream nitrogen blower, which is controlled through a software. The pressure is controlled manually by changing the inlet flow of gas or by pumping vacuum into the sample inside the x-ray hutch at the facility. The pressure can be changed stepwise between 0 bar and 50 bar. The detected two dimensional diffraction patterns are azimuthal integrated into one dimension using the software Bubble. The basal spacing of wet iron bentonites are determined using a D8 Focus diffractometer at the department of material technology at NTNU.

Thermogravimetric analysis is used to determine how dry a clay is. TGA measurements on the water intercalated clays were done with a suitable instrument at NTNU, with a temperature range from 25°C to 200°C or 250°C. At the highest temperature, clays are assumed to be dehydrated, meaning that there should not be any water layers left at this point. In other words, the mass change of a clay sample in a thermogravimetric experiment gives information on how the different clays dry. This is useful for the determination of how hydrated the different clays became while they were measured at 150°C with XRD.

4   Theory

This chapter is a quick introduction to clay minerals. In addition, a few important aspects on x-ray scattering experiments are presented. Most of the information below is reused from my specialization project from December 2022.

4.1   Clay minerals

Clay is a substance most commonly associated with mud. There are many different types of clays that are naturally occurring in soils all over the world. They compose of fine grains that are plastic at appropriate water contents and harden as they dry[10]. Due to this property, it is a well known material used in pottery, but is also useful when building houses, as an ingredient in cosmetics, agriculture, and oil and gas development. Recent studies show that dry clay minerals may be used for carbon capture and storage. Clays contain water in various forms, meaning that water bind to available pores at the surface of a clay mineral. These molecules can be elevated from these sites typically between 100 and 200°C, and is often known as desorption. For simplicity, clay minerals will further be referred to as clays, and specified if they are synthetic or natural.

Natural clays are stacked in sheets in various ways to compose unique structures. This is called random interstratification of clay minerals. As a consequence, a certain clay sample may have a distinct different layer thickness than other samples of the same clay[11]. The natural clay types bentonite and montmorillonite are classified as smectites, and show a hydrated phyllosilicate structure. Smectites are 2:1 phyllosilicates, meaning that a clay layer compose of two tetrahedral crystalline sheets with an octahedral crystalline sheet in the middle as illustrated in figure 1, and stacked on top of one another. Unlike fluorohectorites, which is a type of synthetic smectite where the middle layer is trioctahedral, the natural smectites have a dioctahedral structure sandwiched between the two tetrahedral layers[10]. In a dioctahedral layer, each oxygen or hydroxide ion is surrounded by two divalent cations, like Al^{3+}. The trioctahedral layer has three trivalent cations, for instance Mg^{2+}, surrounding each oxygen/hydroxide ion. Montmorillonites and bentonites are 2:1 smectites with two tetrahedral sheets sandwiching an octahedral sheet for every layer of clay as illustrated. In figure 1, the oxygen ions are represented with white spheres, hydroxide ions are represented with green spheres[15]. A general chemical formula for the unit cell of the montmorillonite is given in equation (1). From the formula, it is clear that natural clays compose mainly of silicates and hydroxides as well as exchangeable cations in the interlayer. The cations are illustrated as blue spheres in figure 1, and are typically sodium or calcium in pure montmorillonites. The interlayer is the free space between each octahedral-tetrahedral-octahedral sheet as illustrated in the figure. This is typically filled with a certain number of water layers, labelled 0WL, 1WL, 2WL, depending on the layer thickness. The first water layer is typically 2 Å, while the second gives an additional 3 Å contribution to the total layer thickness. The total distance that include the three sheets and the water layers is called the basal distance, or d-spacing, of a clay. This distance increase as more atomic groups or cations inhabit the interlayer, which is commonly known as swelling. If a water layer is removed, the basal distance is expected to decrease with the corresponding water layer thickness.

$$(Na,Ca)_{0.3}(Al,Mg)_2Si_4O_{10}(OH)_2 nH_2O \tag{1}$$
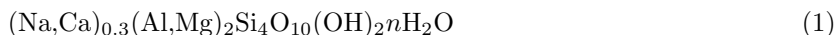
The joining of tetrahedral and octahedral sheets to form a smectite layer results in an electrically negative charged structure, and is typically 0.2 per half unit cell in fluorohectorites and montmorillonites[10]. Tuning the layer charge has proved to be an important factor for optimizing carbon dioxide adsorption in fluorohectorites. The easiest approach to accomplish this is to exchange metallic cations. Lower layer charge allows more accessible adsorption sites for water and CO_2 molecules[6]. Smectites are known for the largest cation exchange capacity compared with other natural smectites, and their interlayers swell more when exposed to CO_2 or water than other types of clay[12]. Bentonite is a type of montmorillonite clay, and is formed from weathered volcanic ash. Bentonite clays have a high cation exchange capacity, compared to other montmorillonites. This clay mineral can adsorb and desorb much more water relative to its own weight compared to other montmorillonites[2]. For this reason, bentonite is expected to be an efficient carbon adsorber. Intercalation is the process when new groups of atoms, like water or CO_2, enter the interlayer between the sheets. This process causes clays to swell, meaning that the d-spacing
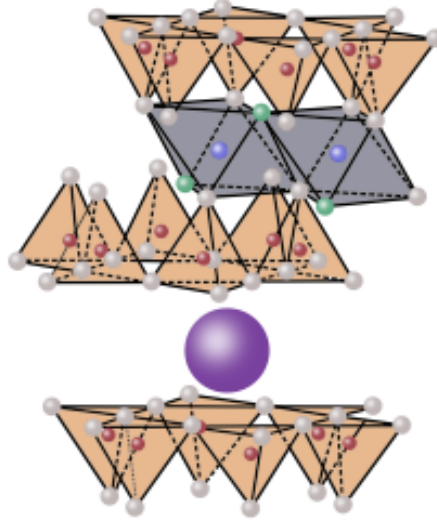
Figure 1: Montmorillonites and bentonites are 2:1 smectites with two tetrahedral sheets sandwiching an octahedral sheet for every layer of clay as illustrated. The interlayers contain cations.

increases.

Cation exchange capacity is a measure of how many positively charged ions a certain type of soil or clay can hold. Decreasing the negative layer charge can be done by exchanging higher charged cations to increase the swelling of the interlayer. Exchanging cations in synthetic fluorohectorite clays is one way for the basal distance to increase once exposed to CO_2. The basal distance in fluorohectorites exposed to CO_2 increases the most in the clays that were cation exchanged with either nickel or iron.[7].

4.2   X-ray diffraction

X-ray diffraction is a useful measurement technique for classifying the crystalline structure of materials. In x-ray diffraction, the constructive and destructive interference of scattered x-rays from the electrons in atoms form a diffraction pattern. These patterns can be used to define crystal structures in materials by comparing characteristic peak positions for different types of atoms and the spacing between them with the obtained pattern.

The wave package of the electromagnetic x-ray photons are generalized as a plane wave on the form

$$\psi(\vec{r}, t) = Ae^{i(\vec{k}\vec{r} - \omega t)}. \tag{2}$$

$\vec{r}$ and t are the spatial and temporal positions of the wave, $\vec{k}$ is the wave vector of the photon. The magnitude is defined by the inverse wavelength $2\pi/\lambda$ of the photon with wavelength λ. ω is the angular frequency. $\vec{k}$ and ω are defined from the input energy of the photon directed from the x-ray source to the material, while A is the amplitude of the plane wave. For simplicity the temporal part of the wave function can be neglected for now. X-ray diffraction is a good method to measure the basal distance in clays at different pressure and temperatures.

The main condition for constructive interference in a scattering experiment is given by Bragg's law. Bragg's law gives the relation between the wavelength of the incident wave, λ, the scattering angle θ and the spacing between crystalline layers, d, in equation (3). The relation is also illustrated in figure 2. Bragg's law is satisfied when two beams scattered from two different lattice points give constructive interference at the detector of nth order, where n is the number of interference spots on the detector between them, forming a diffraction pattern for the allowed theta values where Bragg's law is satisfied. The first strong peak in the diffraction pattern is often referred to as the first order Bragg peak. This

is the first order for constructive interference, and the d-spacing from Bragg's law is the estimated layer distance. Bragg's law is only valid for $\lambda \leq 2d$, so it is important that the photon wavelength is comparable with the size of the layer spacing in the studied material.

$$n\lambda = 2d\sin(\theta) \tag{3}$$
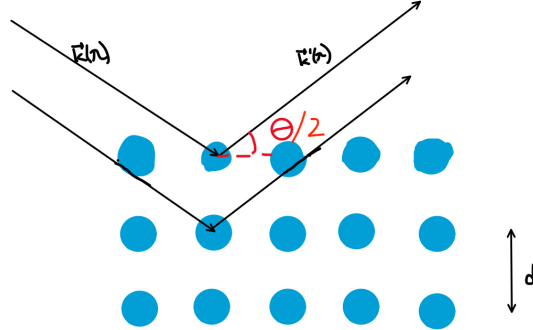
Figure 2: Bragg's law is illustrated for an arbitrary structure where two incident wave vectors $\vec{k}$ are scattered from two different lattice sites at angle θ, the scattered wave vectors are defined as $\vec{k'}$. The two waves hit a detector, and an interference pattern is obtained where the distance between the constructive interference spots correspond to the layering distance, d.

The diffracted intensity is a convolution between the atomic form factor and the structure factor. The structure factor is a measure of how particles in a sample interact with each other. The atomic form factor contain information on the unit cell of the particles located in the sample. The total intensity can also be affected by a thermal contribution called the Debye-Waller correction factor, which increases for higher temperature due to increased interaction between particles. A crystalline structure is defined by a unit cell and the lattice vector $\vec{r_m}$ which is further defined from the primitive lattice vectors $\vec{a_1}$, $\vec{a_2}$ and $\vec{a_3}$ and the Miller indices x_{1m}, x_{2m} and x_{3m}.

$$\vec{r_m} = x_{1m}\vec{a_1} + x_{2m}\vec{a_2} + x_{3m}\vec{a_3} \tag{4}$$

The Miller indices specifies a certain lattice point, m, in the crystal. They also give information about the orientation of one unit cell. The unit cell is a basis of an atomic group that repeats over distances $\vec{r_m}$. The third miller index is used to determine the distance between the planes in layered structures.

When working with scattering experiments, it is more expedient to work in Fourier space rather than in real space. The collection of Laues three equations is the reciprocal equivalence to Bragg's law in real space. The three Laue equations are defined for each Miller index x_i and the primitive lattice vectors $\vec{a_i}$ for an arbitrary lattice site as in equation (4).

$$\vec{q} \cdot \vec{a_i} = 2\pi x_i \tag{5}$$

All three Laue's equations need to be true for diffraction to occur, and is given on general form in equation (5). The solution of the equations describes three different mathematical cones, and diffraction occur at the intersection of these three cones. They can be described graphically with the Ewald sphere in figure 3. The lattice points located at the surface of the 3D sphere, or circumference in 2D, illustrate where diffraction occur. The scattering vector $\vec{q}$ is defined as the difference between the incoming and outgoing beams, $\vec{k}$ and $\vec{k'}$. The scattering experiment is an elastic process, meaning that the total momentum in the process is conserved and the magnitudes of the wave vectors are constant $k = \frac{2\pi}{\lambda}$. As a consequence, the scattering vector is only dependent of the initial, constant wavelength and the scattering angle difference from the experiment. The length of the scattering vector is given in equation (6), and has dimension of inverse length.

$$\vec{q} = \frac{4\pi sin(\frac{\theta}{2})}{\lambda} \tag{6}$$

The expression for basal distance d in equation (7) is obtained by combining equations (3), (5) and (6), while considering the geometrical relations illustrated by the Ewald sphere in figure 3. q_{001} define the q-position for the first order Bragg peak in the diffraction pattern.

$$d = \frac{2\pi}{q_{001}} \tag{7}$$
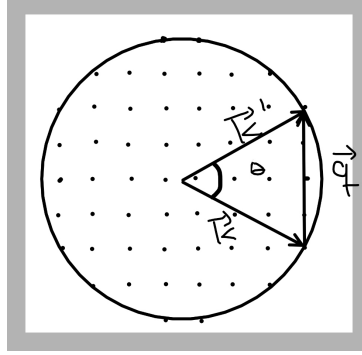
Figure 3: The Ewald sphere is illustrated in two dimensions with incoming and scattered wavevectors $\vec{k}$ and $\vec{k'}$, and the scattering vector $\vec{q}$ between lattice points. The diffraction condition is graphically defined from lattice points located on the surface of the sphere, or circumference of a two dimensional Ewald circle.

The form factor of a particle, $F(\vec{q})$, is defined from the lattice vector $\vec{r_j}$, and the unit cell of the particle $\vec{R_n}$. The expression is given in equation (8).

$$F(\vec{q}) = \sum_{r_j} f_j(\vec{q}) e^{i\vec{q}\cdot\vec{r_j}} \sum_{\vec{R_m}} e^{i\vec{q}\cdot\vec{R_m}} \tag{8}$$

f_j is the scattering amplitude, which is defined by the Born approximation in equation (9). $\rho(r)$ is the electron density in a material.

$$f_j(q) = \int_0^\infty \rho(r) e^{iqr} dr \tag{9}$$

The diffracted intensity can be written as a convolution between an instrumental contribution and sample contribution, as shown in equation (10). h is an arbitrary constant, and depends on the amplitude of incoming x-ray photon. F(q) is the form factor, which is defined as in equation (8). $L_P(q)$ are the Lorentz-polarization factors, and the function is defined for different q with a fixed wavelength λ and number of favorable oriented crystals, ν, for a specific polarization P as in equation (11). ν is typically 0 for perfect crystals, 1 for perfect powders and higher for all other type of structures. Γ can be written as a function of the sample resolution, Ω_L and instrumental resolution, Ω_G as shown in equation (13). q_0 corresponds to the centered q-value at one of the Bragg peaks. η is the mixing factor between the instrumental and sample contribution to the pattern, and is given in equation (14) [14].

$$I(q) = h|F(q)|^2 L_P(q)\Phi(q) \tag{10}$$

$$L_P = \frac{P}{\sqrt{1 - (\frac{\lambda q}{4\pi})^2}(\frac{\lambda q}{4\pi})^{\nu+1}} \tag{11}$$

$$\Phi(q) = \frac{2\eta}{\pi\Gamma(1 + 4(q-q_0)^2} + 2\frac{1-\eta}{\Gamma}\sqrt{\frac{ln2}{\pi}}e^{-4ln2(q-q_0)^2/\Gamma^2} \tag{12}$$

$$\Gamma = (\Omega_G^5 + 2.6927\Omega_G^4\Omega_L + 2.4284\Omega_G^3\Omega_L^2 + 4.471\Omega_G^2\Omega_L^3 + 0.0784\Omega_G\Omega_L^4)^{1/5} \tag{13}$$

$$\eta = 1.36603 \frac{\Omega_L}{\Gamma} - 0.47719 \frac{\Omega_L^2}{\Gamma^2} + 0.11116 \frac{\Omega_L^3}{\Gamma^3} \tag{14}$$

4.3   X-ray generation

There are two primary methods to produce x-rays. X-ray photons are emitted when charged particles change direction or change their velocities fast enough. Electrons are therefore accelerated periodically to satisfy this condition. They can be generated from accelerated electrons inside a synchotron, and directed through beamlines out of the ring. The main advantage to perform measurements at synchotron facilities rather than in a home lab is the many orders increased number of radiated photons. This allow the flux to be relatively high with a good collimation through narrow slits. The increased flux give higher intensity values at the Bragg peaks. The higher peak intensity give sharper x-ray diffraction signal at the Bragg peaks. The powder x-ray diffraction setup at NTNU generates x-rays when high energy electrons decelerate when interfering with the anode inside an x-ray tube. The anode is typically made from copper, but other materials can be used if other photon wavelengths are preferred. Some of the photons are guided though an external tube to the sample, while the majority are wasted immediately after the interaction. The characteristic wavelength is typically between 0.6 Å and 2 Å in an x-ray scattering experiment. The x-ray wavelength is characteristic of the cathode that emits electrons. In a home powder x-ray diffraction lab is the K_α-radiation from copper cathodes typically used. This correspond to a wavelength $\lambda = 1.54$ Å.

5 Experimental section

Two analysis techniques have been used to study montmorillonites and bentonites, both natural, and cation exchanged with either nickel or iron. The procedures of using powder x-ray diffraction and thermogravimetric analysis will be described in this section, as well as the sample preparations done in advance. The description of sample preparation of nickel montmorillonites and the description of the ESRF procedure from November 2022 is reused from my specialization project.

5.1 Sample preparation

Some of the natural montmorillonite and bentonite clay samples are exchanged with nickel and iron(II/III) cations. This is done by mixing the natural clay with an ionic solution containing the relevant cation. In addition, the remaining samples of the clays are left untreated to compare the role of the different cations in the interlayer of clays. Some of the natural bentonite samples were swelled in water for 24 hours before they were cation exchanged with Fe(III) or Fe(II) ions. Other bentonite samples were exchanged with the same cations without pre-swelling in water. All of the samples need to be grounded to fine powder before preparing them in the appropriate container for the different measurement techniques.

5.2 Powder X-ray diffraction

5.2.1 ESRF

The powder x-ray diffraction data of nickel- and natural bentonite and montmorillonite clays were collected at the Swiss Norwegian Beamline 01 at ESRF in Grenoble, France. The diffractometer is based on the PILATUS2M detector, and combines advantages of pixel area detector with flexible goniometry and easy re-positioning of the detector in vertical and horizontal directions. PILATUS@SNBL is controlled by Pylatus software that also supports Oxford Cryostream700+ (80-500K). This software can also be used to program a sequence of diffraction experiments at various conditions[3]. The beam of the x-rays used in the first sequence of diffraction experiments have wavelength $\lambda = 0.77$ Å. Nickel bentonite was remeasured at ESRF with higher photon energy and flux. The x-ray beam size was then $250.37 \times 212.07 \mu m^2$ and photon wavelength $\lambda = 0.605$ Å. The same measurement setup was also applied on a sample of nickel Crook2 montmorillonite clay.

To process the images from the x-ray detector correctly, a scan of a known crystal LaB_6 was done because of its characteristic diffraction pattern. In practise, this is done to calibrate the sample-to-detector distance, l= 500 mm. A general scan of the x-ray beam was done before measuring a new clay sample to optimize the intensity of the incoming and scattered beams. This also ensure that the x-ray source is turned on in the beginning of a new scan series. This can only be performed if we know that the detector will not burn when it receives full power. There are also made scans on an empty capillary tube at vacuum and with CO_2 to calibrate the XRD patterns of the clay powders before analyzing the data in Python.

A few millimetres of fine powdered montmorillonite and bentonite clay powder are loaded in the bottom of a borosilicate glass capillary tube with diameter 0.5 mm[5]. The capillaries are topped with a few threads of glass wool to prevent eventual sample blow back when either vacuum is pumped on the sample or higher pressures are applied. The outside surface of the capillary tubes are glued to a swagelock weld gland by the open end of the tube using a Loctite 3450 epoxy glue, which has a UV curable resin tip at the opposite end of the gluestick. Once the glue is dry, the wider part at the end of the capillary tube is cut off using a diamond knife. The capillary tubes can now be mounted onto the goniometer through a pressure cell. The pressure cell compose of a female nut, a Swagelock VCR tee-connection and two gas inlets. The weld gland is connected to the female nut, which further is connected to the gas inlets through the tee-connection. The goniometer is located between the x-ray source and the detector in the setup. The gas inlets can be connected to a gas handling system or a turbo molecular vacuum pump, and is a useful application for CO_2 experiments[13]. The powder in the capillary tube need to be aligned with the center of the x-ray beam. This was done by carefully adjusting the horizontal and vertical axis of the goniometer while rotating the capillary tube through the built-in ESRF software Pylatus[3]. The aligned

position should preferably be packed with clay grains, in order to maximize the scattered intensity.

The capillary tube should be leak tested with gas before starting a measurement of the clay. This is done by opening one valve at a time, while looking for a noise that will correspond to a leakage in the gas handling system. This is done to make sure that vacuum and gas is pumped correctly into the capillary tube. The clay powders are scanned at temperature T= 27°C, and further heated to 150°C while it is pumped vacuum on. Each scan takes 10 s, and the capillary tube rotates between 0° and 30° around the center of the tube. The temperature is controlled by an Oxford Cryostream nitrogen blower placed a few centimetres above the tip of the capillary tube, furthest away from the goniometer. Vacuum was pumped through the Swagelock Tee with frequency 1500 Hz. Measurements were made continuously at the constant high temperature with vacuum for at least an hour to monitor the evolution of the position and shape of the first order Bragg peak in the azimuthal integrated one dimensional diffraction pattern. The integration was done using the software Bubble and WinPlotr, and are parts of the SNBL toolbox[3]. Once the clay is dry, the sample is cooled slowly back to 27°C. The clay is dry if the Bragg peak positions and the relative intensity I_{00l}/I_{001} remain unchanged as the sample cools down. If the measured d-spacing of a dry sample is above 10 Å, will the clay sample be exposed to pressurized CO_2 with increasing pressure from 0 to 20 to 40 to 50 bar, while continuously scanning at each pressure step to monitor the stabilization of the Bragg peaks. Because the CO_2 adsorption mechanism works best at low temperatures, the temperature is kept at 27°C.

In the second ESRF experiment series, NiCrook2 and NiBentonite were heated under vacuum at 150°C for approximately 3 hours and waited for the first order Bragg peak positions to remain unchanged. This is an indication that the clays are completely dry. They were further cooled down slowly to 27°C, and waited for 10 minutes to check that the peak positions still remain unchanged, since this is a second indication that the sample is dry. The aim of this experiment was to confirm if the clays take up CO_2 at all. For this reason are the two dried samples only exposed to 40 bar of CO_2, with quality 99.998% for 52 minutes. Crook2 was also measured with 1 and 0 bar CO_2 to observe how the diffraction pattern change when decreasing the pressure of carbon dioxide.

5.2.2 D8 Focus

Iron and nickel cation exchanged and natural bentonites were measured with a Bruker D8 Focus powder x-ray diffractometer. This instrument generates CuK_α-radiation with wavelength $\lambda = 1.54$ Å, and consist of a LynxEye™ SuperSpeed Detector. The samples are prepared in silicon cavities with diameter 15 mm, and further inserted into dome holders. Finally, the dome holders are loaded onto one of the nine stages in the instrument, scanned with 0.75 s exposure time at every θ-values between 4° and 30°, with step size 0.008°. The x-ray beam is collimated by inserting a 0.2 mm wide slit between the x-ray tube and the sample.

The preparation of dried clays are done inside a dry, concealed glove box where the humidity is less than 5%. The samples are further left on a heating plate with 150°C to dry for at least 24 hours. The dry clays were inserted into the same silicon cavities and dome holders before they were taken out of the glove box, in order to avoid any unwanted water interaction from the ambient humidity coming from the water concentration in air. The dome holders are used to keep the samples dry while they were scanned. To obtain comparable results, it is necessary to measure the wet clays in dome holders as well, even though they do not require preparation in an environment with strictly controlled humidity. The D8 Focus powder x-ray diffractometer did not support mounting capillary tubes with the pressure cell, in contrast with the x-ray diffractometer at ESRF. In other words, it was not possible to measure pressurized clays in this setup. Hence, only wet and dry clays were measured in this setup, and the clays should be sent to a synchotron to obtain sharper signal when measuring CO_2 intercalated clays.

5.2.3 Data handling

The data collected from the diffractometer at ESRF are preprocessed with SNBL Tool Box and then treated with Bubble[3]. The intensity data points are plotted with respect to the scattering vector q in a two dimensional diffraction pattern in Bubble. This can further be azimuthal integrated to a one dimensional function using WinPlotr, which is part of the same tool box. The Python plotted intensity
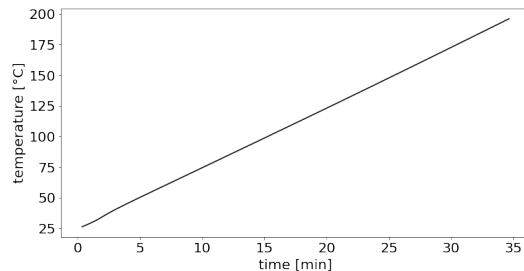
Figure 4: Thermogravimetric measurement method 1 involves measuring the mass and the mass change in a sample while heating it from 25 to 200ºC with heating rate 5ºC/min.

has subtracted the intensity signal obtained from the empty capillary scans. The d-spacing for each measurement scan can be determined from the scattering vector at the first order Bragg peak position and the relation in equation (7). The maximum intensity is directly read out from the plot, and depends on the sample- and beam size. q_{001} is the position of the first order Bragg peak from the different integrated diffraction patterns.

The one dimensional diffraction patterns from Bruker D8 Focus are interpreted using the software Diffrac.EVA. The software has a built in function which calculates the layer spacing from the θ values in the detected diffraction pattern to obtain a basal distance dependent diffraction pattern. The data is further handled in Python, where the signal from the dome holder is subtracted from the signal of the sample, after scaling the background intensity signal to be the same in both data sets.

5.3   Thermogravimetric analysis

Thermogravimetric analysis is a measurement technique used to determine how the mass of a sample changes under heating. It is a useful tool to estimate the water content in clays, and therefore the likelihood for the clay samples heated to 150ºC in the x-ray diffraction experiments to be completely dry. The TGA measurements were done with a Mettler tga/sdta851e instrument. The setup includes a cooling system with circulating water to make sure that the instrument do not burn, but is also useful to efficiently cool down the sample and the instrument. A flow of nitrogen need to be applied through the tube where the sample is located as well. Another feature of the setup is a pan within a furnace tube inside the TGA box, where the sample is loaded. The pan is connected to an analog mechanical scale, which communicate with the software METTLER STARe to digitize the mass measurements. A new measurement of the mass is obtained once every second. White alumina crucibles are filled with powdered clay, and inserted in the middle of the pan. As the temperature increases, the mass decrease with a rate dependent of the water content in the interlayers of the different clays as well as their ability to desorb water. The thermogravimetric analysis is first done on wet clays that are heated from 25ºC to 200ºC with a rate of 5ºC/min. The other set of measurements were done on bentonite and Crook2 montmorillonite clays heated from 25ºC to 250ºC with the same rate as before, and kept fixed at the highest temperature for 30 minutes. Finally, the mass was also measured while the sample cooled down to 25ºC at rate −5ºC/min.

Samples of the nickel exchanged and natural montmorillonites Gonzales and Crook1, bentonite and hydrobentonite were prepared in clean aluminum crucibles. The crucibles are left inside a desiccator with 43% relative humidity at room temperature for at least 48 hours. The humid environment is prepared by inserting a dish with saturated potassium carbonate solution in the bottom of the desiccator. This is done for the samples to be more comparable with the TGA results on synthetic nickel fluorohectorites[8]. They are finally put on a thermogravimetric analysis measurement from 25ºC to 200ºC. The end temperature is set slightly higher than the previous defined dehydration temperatures between 38 and 173ºC for natural montmorillonites[16], to make sure that the samples are well dehydrated at the end of each measurements. New samples of nickel- and natural bentonite were measured a second time with TGA within the temperature interval 25ºC and 250ºC. These were prepared in the same way as the samples from the previous sequence. Iron bentonites, NiCrook2 and natural Crook2 have been prepared and kept in the desiccator for 24 hours as well, before they were put onto the same TGA procedure.
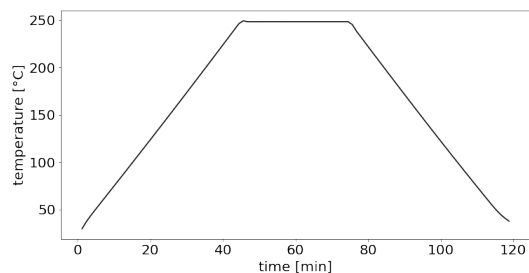
Figure 5: Thermogravimetric measurement method 2 involves measuring the mass and the mass change in a sample while heating it from 25 to 250°C with heating rate 5°C/min, keeping the temperature fixed for 30 minutes and cool it down to 25^0C with cooling rate -5°C/min.

5.3.1 Data handling

The temperature dependent mass is plotted with the STARe software, which is connected to the thermogravimetric analyzer through Bluetooth. This is the most common software used for thermogravimetric analysis, and allows the user to consider the time dependent mass and its derivative. The temperature dependent mass can also be plotted in the software. In addition multiple curves for different powders can be plotted together. This is useful when studying the influence of nickel or iron intercalation in clays, or to compare drying in different clay types. To further compare the relative mass change, a Python script is applied on the data set to compute the percentage of the mass of each dehydrated clay, and plot the curves for the different clays in the same window at comparable scales.

6 Results

In the following section, the data collected from the instruments described in the previous section is presented in figures and tables. The XRD data on Crook1, Gonzales and the first set of bentonite were also included in my specialization project.

6.1 Nickel montmorillonites and bentonites

6.1.1 Powder X-ray diffraction

In the following subsection, the integrated intensity plots of x-ray diffraction patterns and the calculated layering distances for the nickel cation exchanged montmorillonite and bentonite clays, measured at different pressure and temperature are presented in figures below. The two dimensional diffraction patterns obtained from the measurement scans at ESRF looks similar to the one illustrated in figure 6, which is a scan of wet nickel-Gonzales. The diffracted intensity signal from the first order Bragg peak align with the half ring with radius 500μm. The first ESRF measurements on natural smectites, were obtained in November 2022 and are also included in my specialization project. The second series were obtained from ESRF in May 2023, and focused on intercalation with carbon dioxide in nickel bentonite and nickel Crook2 montmorillonite.
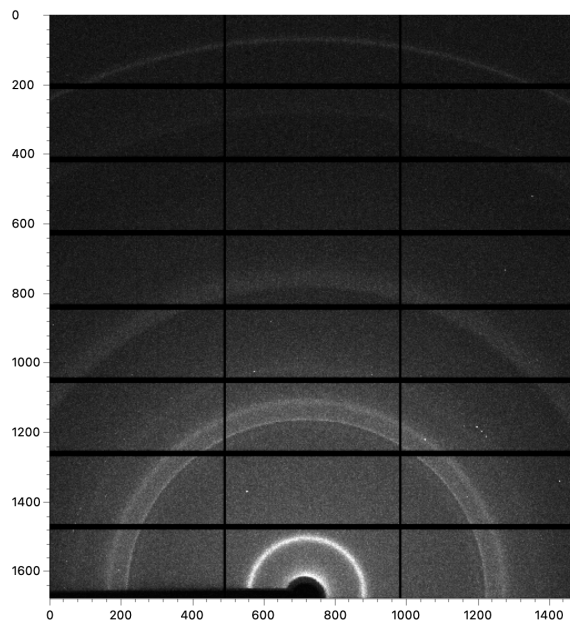
Figure 6: The 2D X-ray diffraction pattern of wet nickel Gonzales. The image is used as an example plot, and the two dimensional diffraction patterns are integrated from a similar image using Bubble.

The following figures present the measured data from the first ESRF measurement sequence on nickel bentonite. This include a measurement of dry bentonite to compare the contribution of nickel cations to the layer spacing. A zoomed plot of the first order Bragg peak in the integrated diffracted intensity plot from the scans done when drying the clay and later applying increasing pressure, is illustrated in figure 7. The scan of the cold and wet powder was done at another position in the capillary tube than the other measurement because of motion of powder within the tube when the vacuum pump was turned on. This is the main reason why the intensity signal is much bigger compared with the other scans. The diffraction plots from the scans for decreasing pressure are presented in figure 8. The mean q-value at the first order Bragg peak increase when the powder is drying and decrease as the carbon dioxide pressure increases. The changes in peak position at different pressures and temperatures are clearly defined for the first order Bragg peak. The q-value for the first order Bragg peaks increase when the powder dries, while the intensity decreases and the peak width become more narrow. Zoomed plots of the third order Bragg peaks at different pressure and temperature are presented in figure 9. The signal at the third order Bragg peak is very weak, and the change in intensity, width and q-position for this peak is poorly

defined. In other words, the higher order peaks are not helpful to determine any structural change of CO_2 exposed nickel bentonite.

When CO_2 is applied on the sample, nickel bentonite starts to swell. This is illustrated with a decreasing q-value for the Bragg peaks. The Bragg peak widths broaden and their corresponding intensity increases. The peak is asymmetric with a left shoulder at the first order Bragg peak for higher pressure and low temperatures. The shoulder's intensity increases and q-value decreases as the pressure increases. An opposite change of the peak shape and position occur when the pressure decreases. The diffraction pattern of the reheated sample with pumped vacuum aligns well with the one for the dried sample. The dried natural bentonite sample, which has not been exchanged with nickel cations has a narrow peak with a higher q-value compared with the measurements of nickel bentonite. The q-value corresponds to a d-spacing 9.67 Å, and is therefore too low to take up CO_2. The d-spacing is determined from equation (7) by inserting the q-value for each first order Bragg peak, and are listed correspondingly in table 1 for the correct temperature and pressure combination and measurement order. The measured data for bentonite without any nickel cations(MNT) is used as a reference to determine the role of nickel cations in natural clays. The shoulder peak in the diffraction pattern for the pressurized clay samples is here illustrated with a second value for the layer spacing. The shoulder indicate that only half of the layers in bentonite expand in response to CO_2. The lowest d-spacing value correspond to the bentonite sample without nickel. The full width at half maximum for the double peaks are determined from a saddle point between the two peaks as the middle, resulting in a bigger value compared with the single peak widths. The heating of another sample of the bentonite powder had previously been measured, where the layering distance decreased from 13.54 Å to 10.46 Å. The sample exploded after 37 bar CO_2 was applied. For this reason is a new bentonite sample, prepared from the same powder and heated under similar conditions, measured when exposed to a step-wise increase in pressure. This is one reason for the difference in intensity values. The pressure hysteresis plot of the d-spacing in bentonite with respect to CO_2 pressure is shown in figure 10. The vertical line at 0 bar correspond to the sample drying at 150°C while pumping vacuum.

The results from the second ESRF experiments with nickel bentonite are presented in the following figures. Figure 11 show the normalized diffraction patterns zoomed in at the first order Bragg peak for different temperature and pressure specified in the graph. The Bragg peaks are marked with "x"'s, and labelled with the calculated d-spacing according to equation (7). The broadening of the peak indicate that not all of clay layers have been cation exchanged. The change in d-spacing while drying the clay with respect to time is illustrated in figure 12 while figure 13 show that the d-spacing barely changed after the clay was exposed to 40 bar CO_2. The values of the d-spacing from the second ESRF measurement are included in table 1. The d-spacing decrease from 14.31 Å to 10.13 Å while NiBentonite is heated, and increase to 10.15 Å when exposed to 40 bar CO_2.

Table 1: The measured d-spacing for temperature and pressure cycle of nickel bentonite and dry bentonite at ESRF. The two colums for $d_{1,2}$ indicate if the meaurement was performed in November 2022(1) or May 2023(2).

temperature [°C]	pressure [bar]	d_1[Å]	d_2[Å]	Ni/MNT
27	0	12.5	14.31	Ni
27	0	12.5	10.72	Ni
150	0	10.92	10.04	Ni
27	0	10.36	10.13	Ni
27	20	11.55, 10.34	-	Ni
27	40	11.91, 10.33	10.15	Ni
27	50	12.41, 10.54	-	Ni
27	2	12.03, 10.51	-	Ni
27	0	11.73, 10.46	-	Ni
150	0	10.30	-	Ni
150	0	9.67	-	MNT

The one dimensional diffraction pattern for Gonzales montmorillonite, zoomed in at the first order Bragg peak, is presented in figure 14. The intensity decreases and the width broaden when the powder is drying, and reverse once it is pressurized with CO_2. The q-value for the Bragg peaks increase when drying, and decrease once the sample is exposed to CO_2. The Bragg peaks of second, third and fourth order are presented in figure 15, normalized to the maximum intensity of the first order peak. There is some
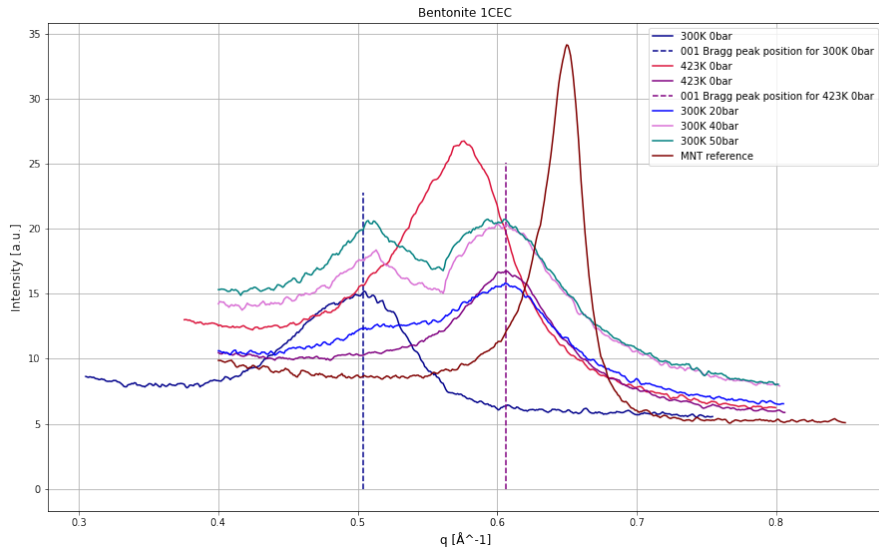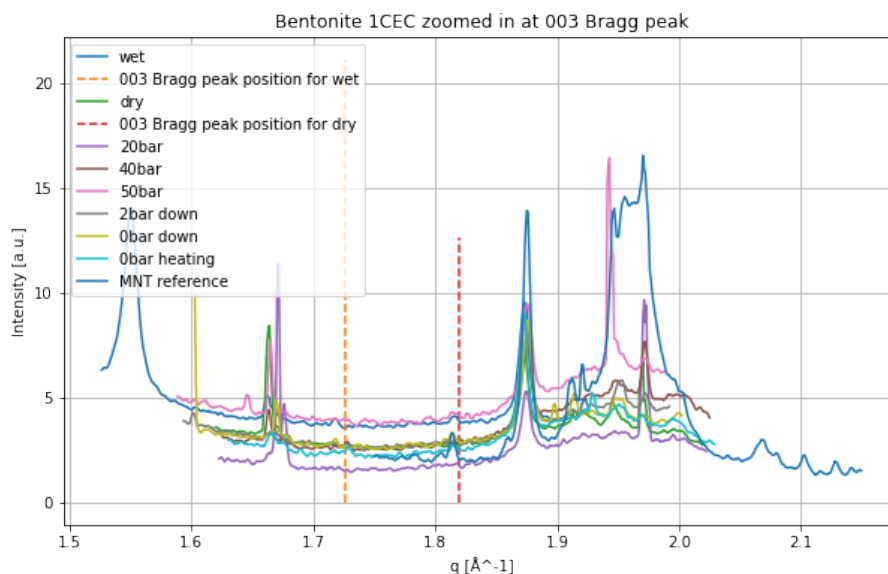
Figure 7: The zoomed plot around the first order Bragg peak for drying bentonite, and increasing the pressure of carbon dioxide going into the sample. The scan of the dried natural bentonite in green shows a layer spacing significantly lower compared with nickel exchanged bentonite. The XRD data was obtained from the first ESRF sequence.
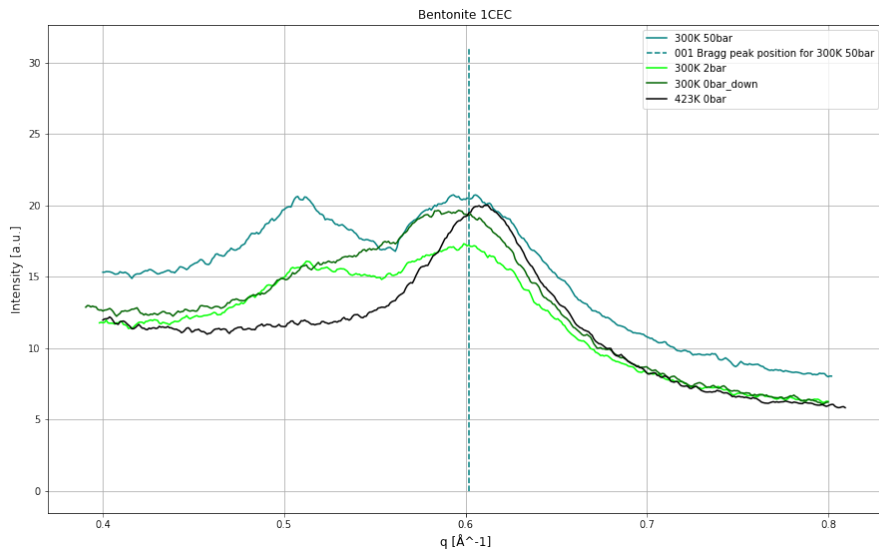

Figure 8: The zoomed plot around the first order Bragg peak for bentonite at decreasing pressure. The sample was reheated once the pressure was 0 bar again. The XRD data was obtained from the first ESRF sequence.

broadening at the third and fourth order peaks of the pressurized powder compared with the wet powder, while the signal at the second order peaks are flat. The broadest peaks were detected in the driest powder, illustrating that the different clay grains have different interlayer distances. The interlayer spacing at different pressures and temperatures are presented in table 2, along with their corresponding measured intensity. The d-spacing is plotted with respect to pressure in figure 16, showing that it decreased by 0.293 Å when drying at 0 bar, and increased by 0.07 Å after the sample has been cooled down to room temperature, and an additional 0.1 Å after 41 bar of CO_2 has been applied.

Figure 9: Zoomed plot around the third order Bragg peak for bentonite at different pressure and temperature. The XRD data was obtained from the first ESRF sequence.
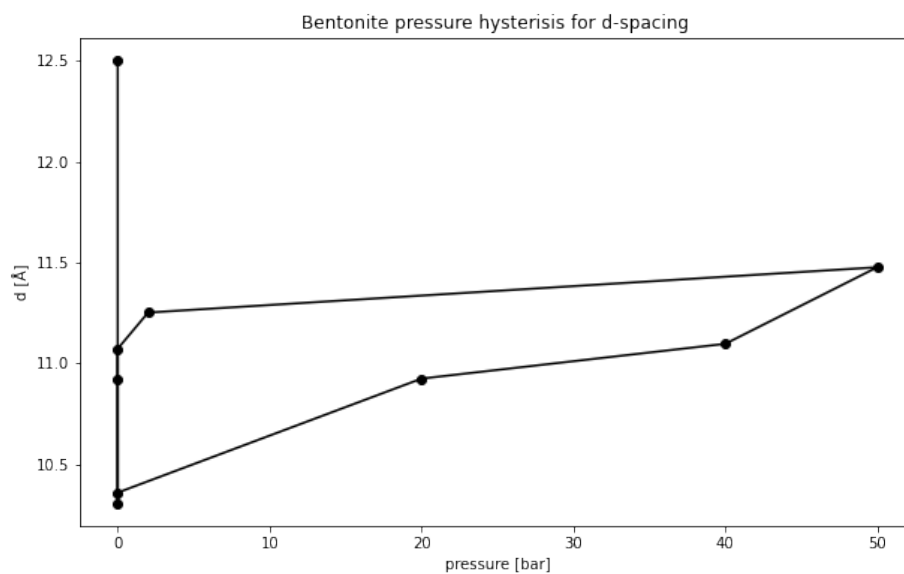

Figure 10: The evolution of the interlayer spacing in nickel bentonite with varying pressure of CO_2. The XRD data was obtained from the first ESRF sequence.

Table 2: Measured d-spacing for the pressure cycle of the montmorillonite Gonzales cation exchanged with Ni^{2+}

| temperature [°C]	pressure [bar]	d-spacing[Å]
27	0	14.02
150	0	13.73
27	0	13.80
27	41	13.90

The nickel cation exchanged Crook1 montmorillonite was measured dry, and afterwards at different pressures. A zoomed plot at the first order Bragg peaks in the diffraction patterns from the different
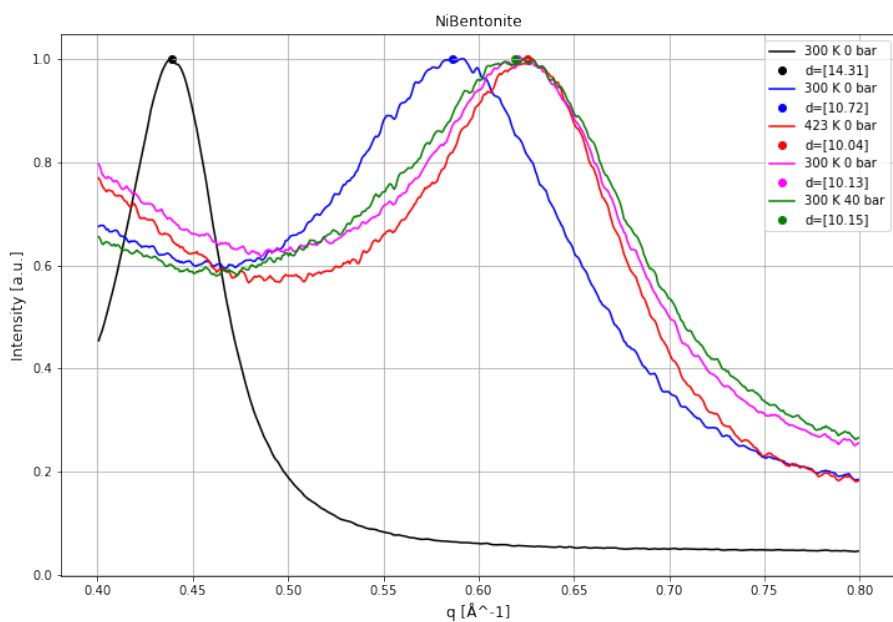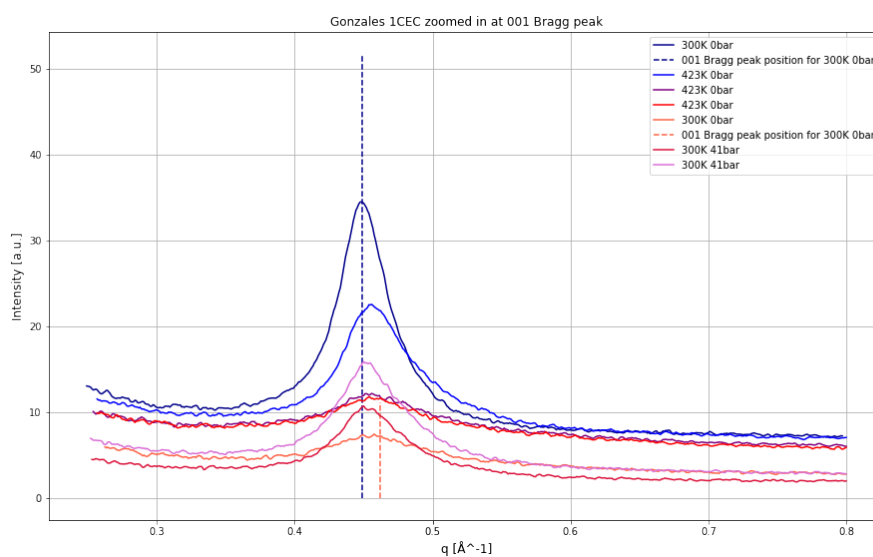
Figure 11: The zoomed plot around the first order Bragg peak for drying bentonite, and when exposed to 40 bar CO_2. The intensity has been normalized with respect to the maximum intensity. The estimated d-spacing has been given, according to the respective q-values of the first order Bragg peaks and equation (7). The XRD data was obtained from the second ESRF sequence.
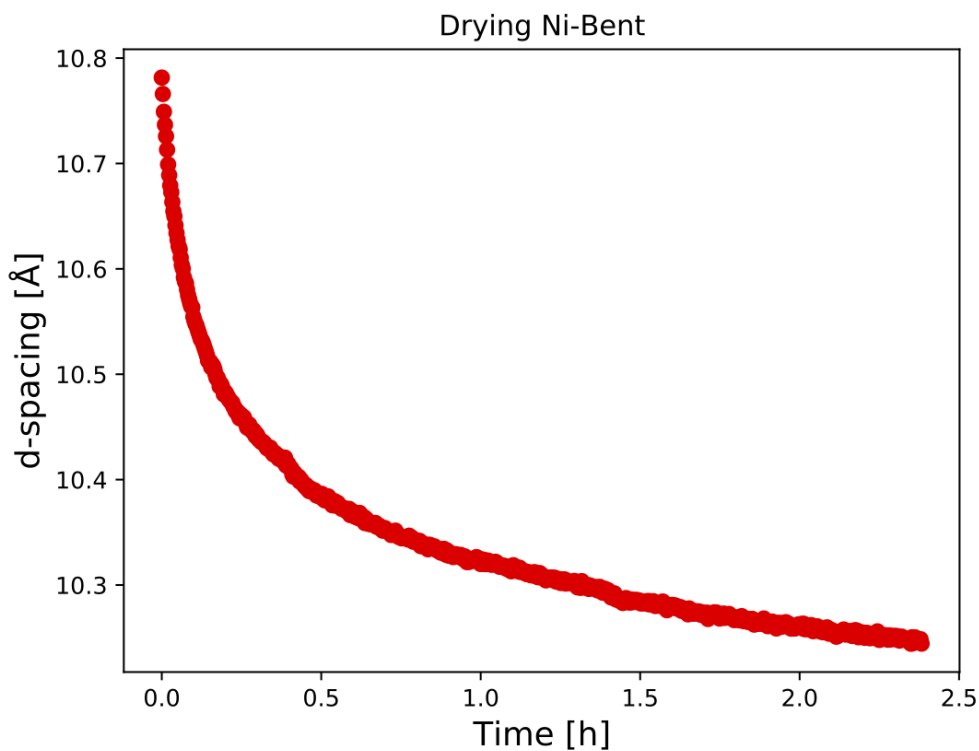
Figure 12: The plot show how little the d-spacing varies with time while the clay was drying. The XRD data was obtained from the second ESRF sequence.
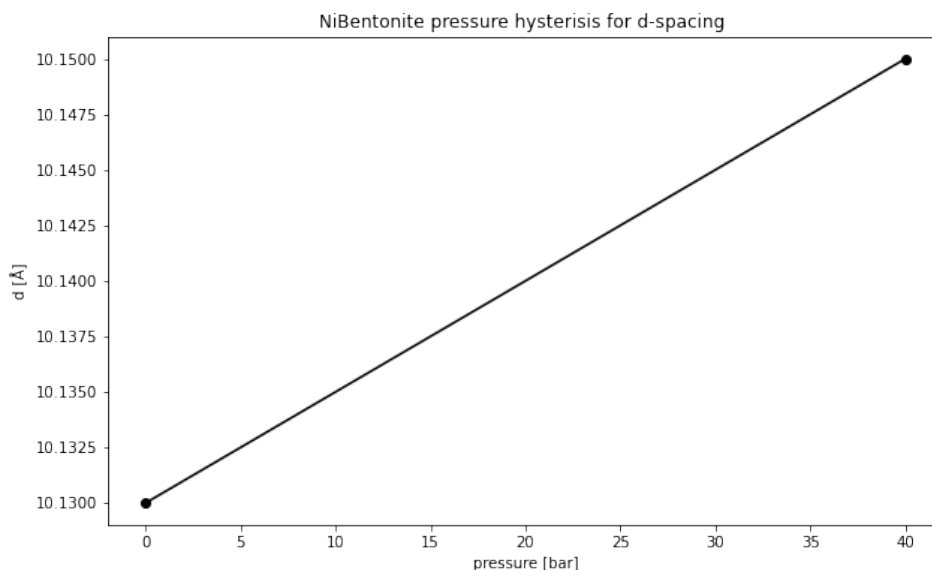
Figure 13: The plot show how the d-spacing changed as the dried clay was exposed to CO_2. The XRD data was obtained from the second ESRF sequence.


Figure 14: The zoomed plot around the first order Bragg peak for Gonzales at different pressures and temperatures show that this peak broaden with smaller maximum intensity when the sample is drying, and reverse the peak change for increasing pressure. The position of the first order Bragg peak does not change much.

scans are presented in figure 17. The basal distance of the dry nickel Crook1 montmorillonite is d≈ 10.3 Å, which is roughly 1WL smaller than when it was wet. The interlayer swelled with Δd≈ 0.3 Å after 50 bar CO_2 have been applied. The plot of the d-spacing for different pressure in figure 18 shows that the changes are smaller compared with the bentonite d-spacing.

The nickel cation exchanged Crook2 montmorillonite was measured dry, and afterwards at different pressures. A zoomed plot at the first order Bragg peaks in the diffraction patterns from the different scans are presented in figure 19. The basal distance of dried Crook2 is d≈ 10.3 Å, which is almost 2WL smaller than wet Nickel Crook2. The decreasing d-spacing in drying NiCrook2 is illustrated in figure 20.
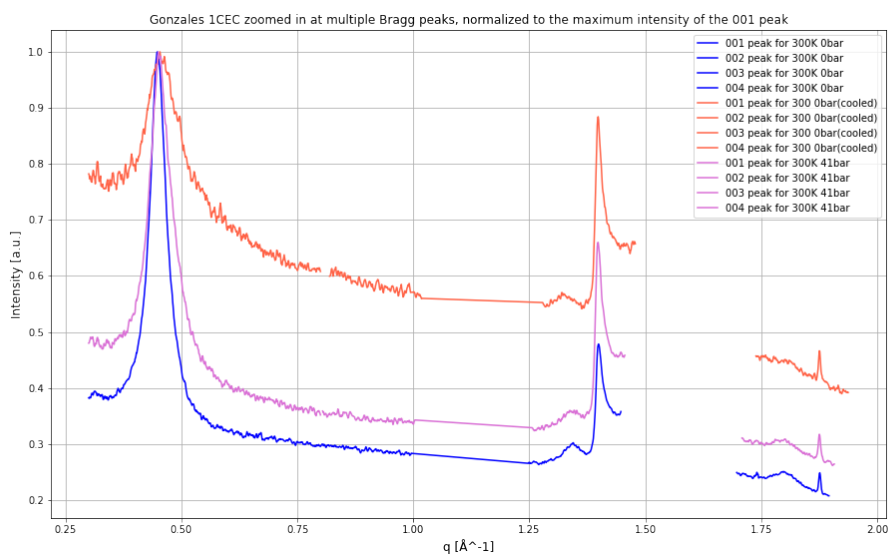
Figure 15: The zoomed plot of the third order and fourth order Bragg peaks with relative intensities to their corresponding first order Bragg peaks from each measurements. The Bragg peak is sharper with narrower peak widths and higher relative intensity for the wet and pressurized sample compared with the dry sample.
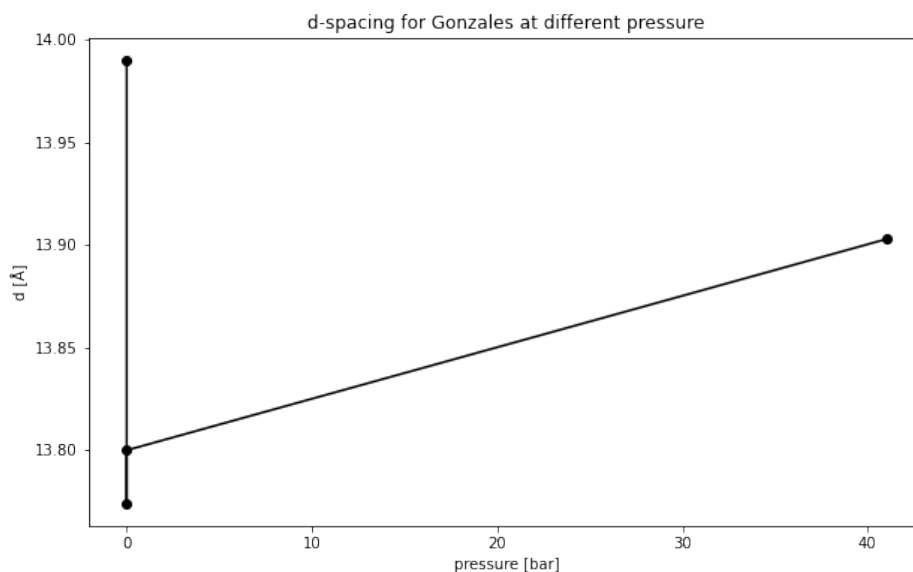
Figure 16: The interlayer distance is plotted with respect to pressure. The scan of the wet sample show the highest d-value, and the lowest come from the driest sample. The slightly increasing d with increasing pressure show that Gonzales take up some CO_2.

Here it is very distinct that there were two water layers in wet NiCrook2, and none in the dry powder. The interlayer increases with $\Delta d \approx 2$ Å after 40 bar CO_2 have been applied at 27°C. This is illustrated with a second shoulder in the diffraction pattern. The plot of the d-spacing for 0 and 40 bar in figure 21 shows that it changes more compared with the new measurements of the d-spacing in bentonite. Table 4 show the d-spacing corresponding to the first order Bragg peaks from the different XRD scans.

The nickel cation exchanged hydrobentonite was measured dry, and afterwards at different pressures. A zoomed plot of the first Bragg peak in the diffraction patterns from the different scans are presented in
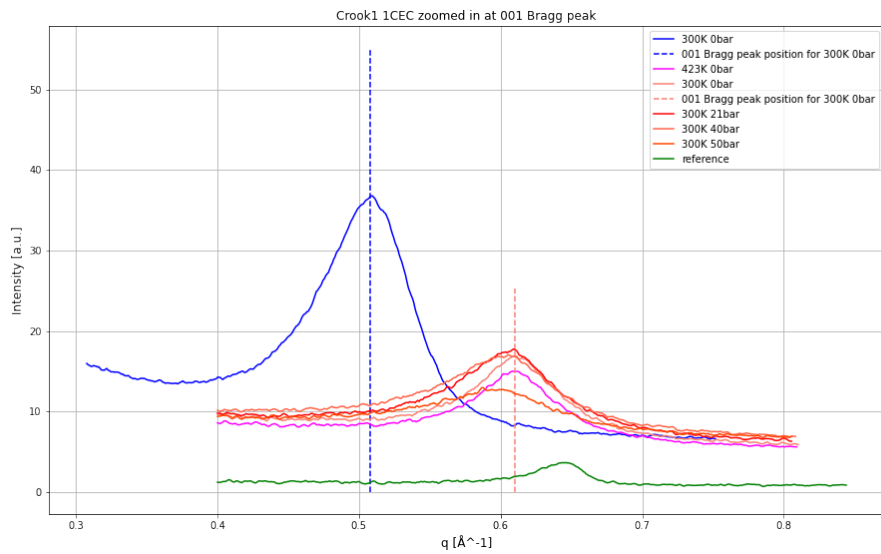
Figure 17: The diffraction pattern of Crook1, scanned at different temperatures and pressures, zoomed in at the first order Bragg peak. In this plot, the temperatures are given in Kelvin.
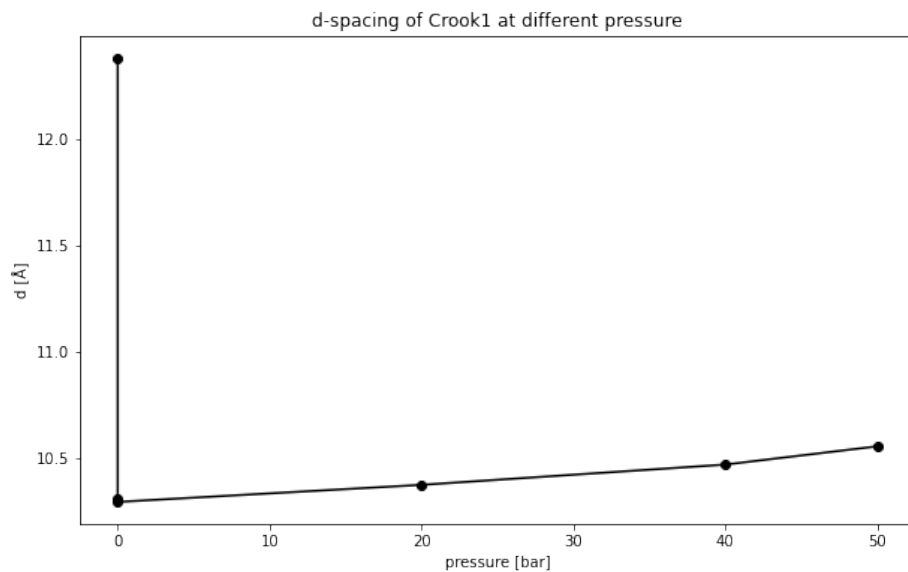

Figure 18: The interlayer distance is plotted with respect to pressure. The scan of the most wet sample show the highest d-value, while the lowest value was measured in the driest sample.

figure 22. The basal distance of the dried nickel hydrobentonite is d$\approx$ 10.3 Å, which is between 1WL and 2WL bigger compared with the wet sample, just like the case for drying NiBentonite in the second measurement. The interlayer swelled with Δd$\approx$ 0.35 Å after 48 bar CO_2 was applied on the clay. The plot of the d-spacing for different pressure in figure 23 shows that it changes more compared with the d-spacing in bentonite from the second measurement. The change in the d-spacing with applied pressure is also slightly bigger than in Gonzales and similar to Crook1.

19

Table 3: Measured d-spacing for temperature and pressure cycle of the nickel montmorillonite Crook1(Ni) and dry Crook1(MNT) at 27°C and 0 bar.

temperature [°C]	pressure [bar]	d-spacing[Å]	Ni/MNT
27	0	12.38	Ni
150	0	10.31	Ni
27	0	10.30	Ni
27	21	10.38	Ni
27	40	10.47	Ni
27	50	10.56	Ni
27	0	9.75	MNT
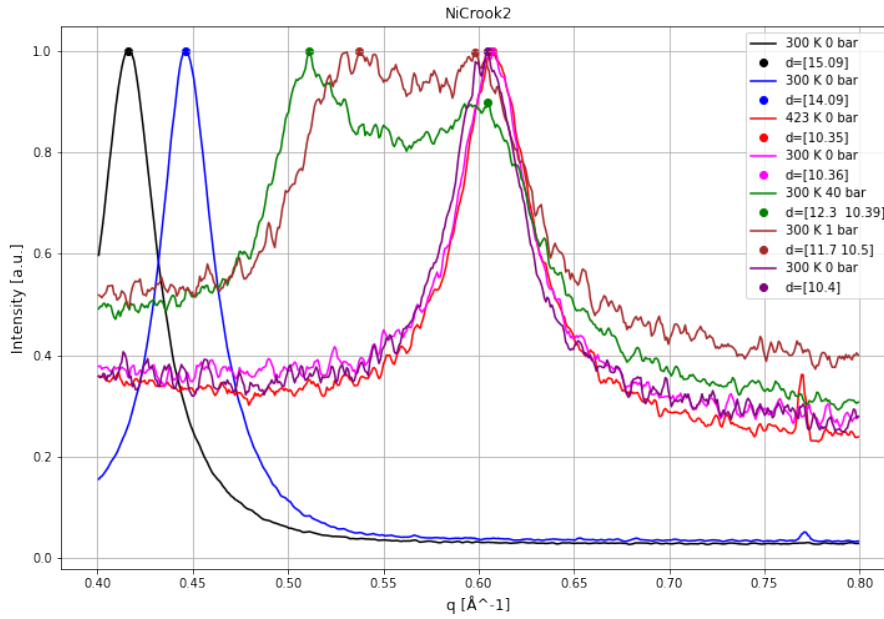
Figure 19: Normalized diffraction patterns of Crook2 relative to the maximum intensities at the first order Bragg peaks, scanned at different temperatures and pressures, zoomed in at the first order Bragg peak. In this plot, the temperatures are given in Kelvin. The Bragg peaks are labelled with the estimated d-spacing, according to their respective q-value and equation (7).

Table 4: Measured d-spacing for different temperature and pressure of nickel montmorillonite Crook2(Ni), together with the d-spacing for dried, natural Crook2(MNT).

temperature [°C]	pressure [bar]	d-spacing [Å]	Ni/MNT
27	0	15.09	Ni
27	0	14.09	Ni
150	0	10.35	Ni
27	0	10.36	Ni
27	40	12.30, 10.39	Ni
27	1	11.70, 10.50	Ni
27	0	10.30	Ni
27	0	9.82	MNT

6.1.2 Thermogravimetric analysis

In this section, the results from the thermogravimetric measurements of nickel- and natural montmorillonites are presented in the following figures. Most of the montmorillonites were measured with a temperature profile described in figure 4. The montmorillonites measured at the second ESRF sequence
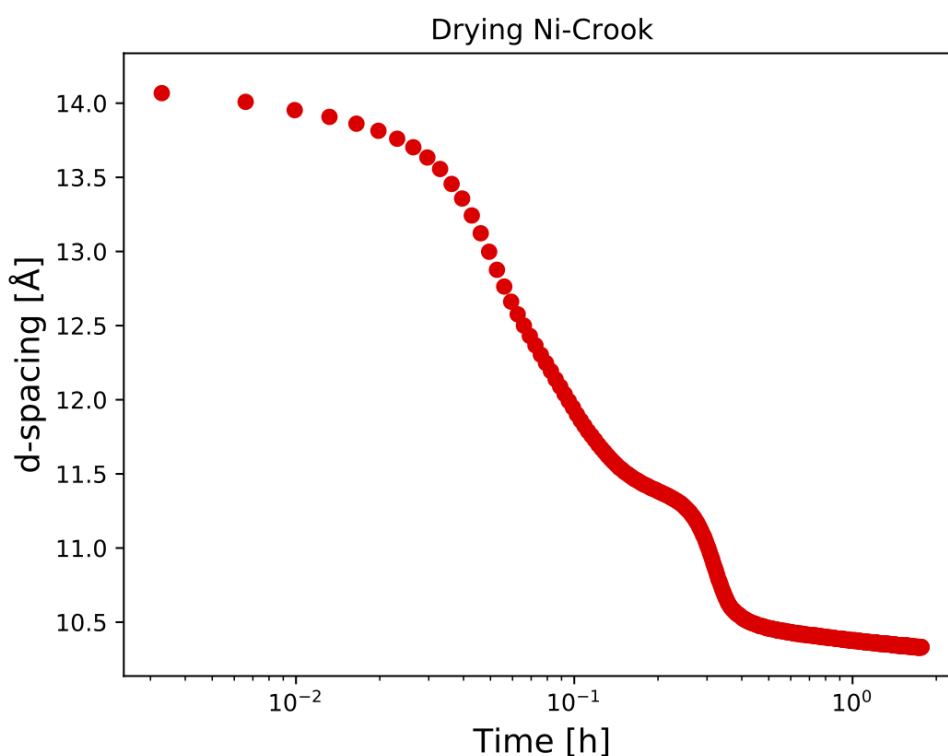
Figure 20: The interlayer distance is plotted with respect to pressure. The scan of the most wet sample show the highest d-value, while the lowest was measured in the driest sample.
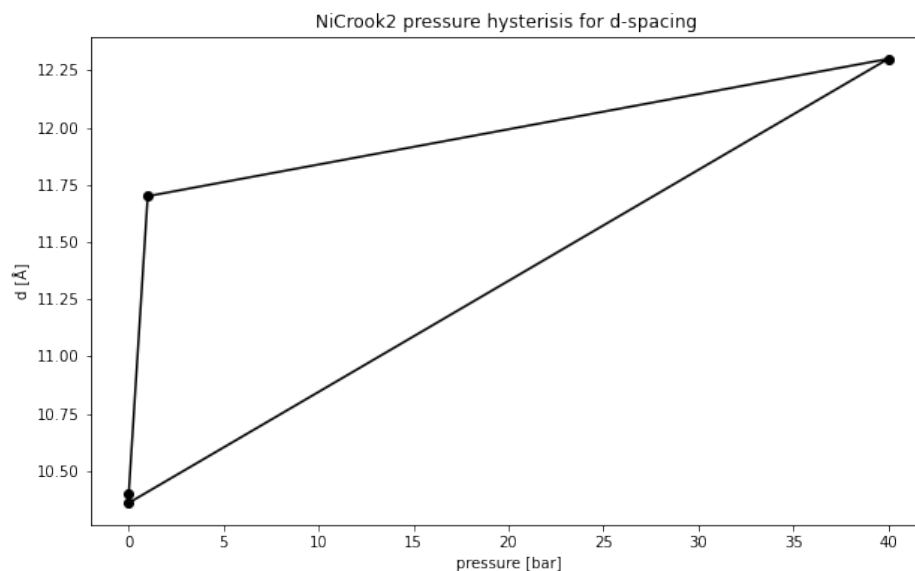
Figure 21: The interlayer distance is plotted with respect to pressure. The scan at 40 bar has the highest d-value, while the lowest value was measured at 0 bar.

were analyzed with a temperature profile described in figure 5 in the TGA instrument. The mass change in the samples when the temperature was fixed at 250°C or during the cooling phase is a defect from the instrument, and is not related to the structural properties of the clays. Therefore only the mass change in response to increasing temperature up to 250°C will be further considered for.

Figure 22: The diffraction pattern of hydrobentonite, scanned at different temperatures and pressures, zoomed in at the first order Bragg peak. In this plot, the temperatures are given in Kelvin.
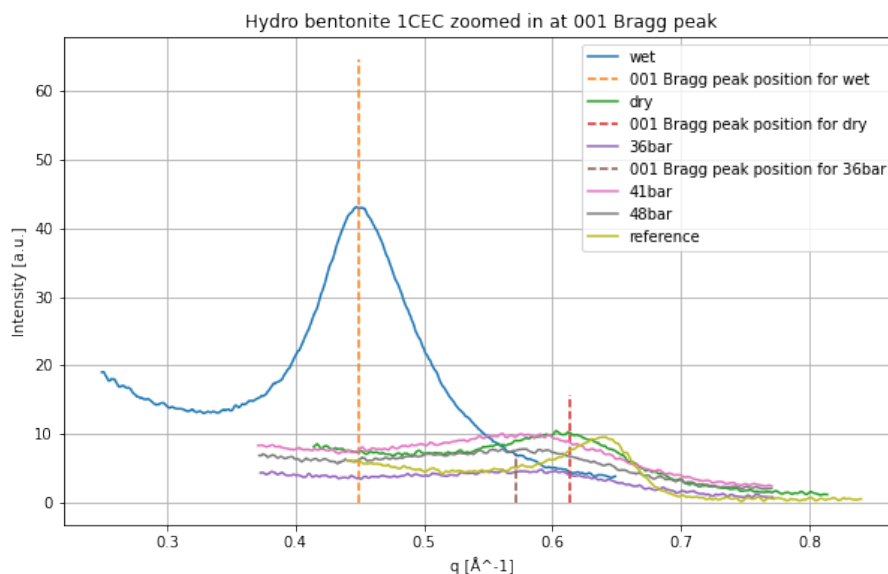

Figure 23: The interlayer distance is plotted with respect to pressure. The scan of the most wet sample show the highest d-value, while the low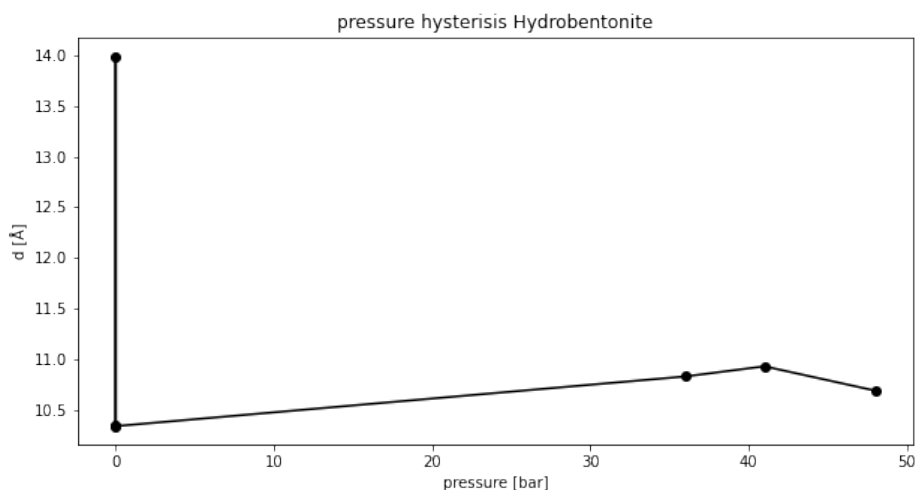est was measured in the driest sample. The vertical line correspond to the change in d-spacing when the clay dried at 0 bar.

Table 5: Measured d-spacing for temperature and pressure cycle of nickel hydrobentonite(Ni) and dry, natural hydrobentonite(MNT).

temperature [°C]	pressure [bar]	d-spacing[Å]	Ni/MNT
27	0	13.99	Ni
150	0	10.35	Ni
27	0	10.34	Ni
27	36	10.83	Ni
27	41	10.93	Ni
27	48	10.69	Ni
27	0	9.85	MNT
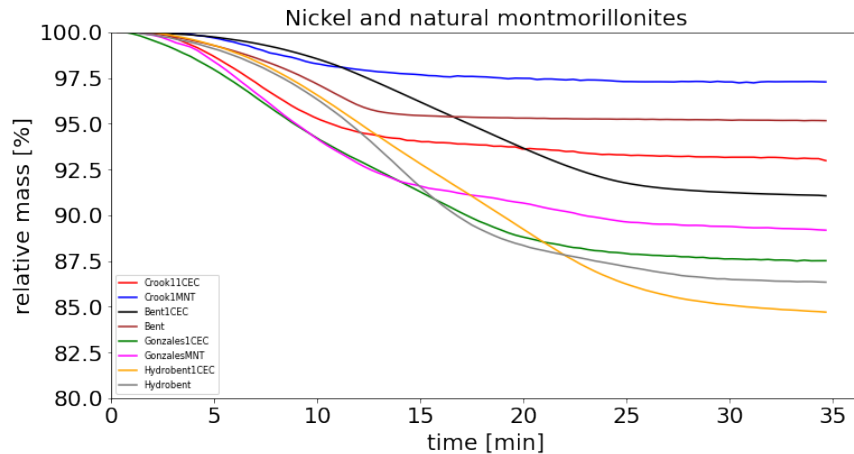
Figure 24: The thermogravimetric analysis plot of both natural and nickel cation exchanged clays shows how the relative mass evolve when heating the samples according to TGA method 1 as illustrated in figure 4.

Figure 24 shows that the nickel exchanged clays generally desorb more water than the natural clays when they are heated to 200°C, as described in figure 4. This is illustrated with a bigger loss in relative mass for increasing sample temperature. Bentonite and Crook1 montmorillonite are the clays that desorb the least, and are therefore considered the easiest to dry. In the TGA plot, this is illustrated with a flat curve for sample temperatures between 100°C and 200°C in Crook1. Similarly, the TGA plot of bentonite shows no mass loss when the sample temperature is above 140°C. Hydrobentonite and Gonzales montmorillonite seem to be the most hydrophyllic, and keep the adsorbed water at the highest temperature. They are also the clays that have the biggest relative mass loss at the end of the measurement.

All of the nickel cation exchanged montmorillonites appear to be dry above 175°C, according to the TGA derivative plot. Figure 25 show how the derivatives of the TGA plots in figure 24 vary in the different montmorillonites. The montmorillonites desorb most water while the sample temperature is between 50 and 75°C. The bentonites desorb most water while the sample temperature is between 75 and 125°C. The nickel exchanged clays seem to have multiple main mass loss rates, while the natural have one main mass loss rate. This suggest that their structure is complex, confirming that not all the layers are cation exchanged with nickel.

The derivatives of nickel Crook1 and nickel Gonzales share the same shape and values below 75°C with a common global minimum at 62.5°C and $-1.0\%/$°C. For higher temperatures, the mass loss rate in Crook1 is close to zero while it is just below $-0.5\%/$°C in Gonzales. The derivative plot for natural Crook1 and Gonzales share the same shape, but the global minimum for natural Gonzales is twice as big as Crook1. They are both close to zero above 150°C. The derivative plot for nickel exchanged bentonite and hydrobentonite share the same form, and both have a global minimum around $-0.5\%/$°C at 150°C. While the derivative plot of nickel exchanged bentonite and hydrobentonite share the same path for temperatures below 100°C, the mass loss rate is significantly smaller in nickel bentonite than in the other.

The TGA measurement of NiCrook2 in comparison to NiBentonite, natural Crook2 and bentonite is shown in figure 26. According to this plot, nickel bentonite desorb water faster than nickel Crook2. The TGA curves for the two nickel exchanged clays are overlapping for all temperatures below 100°C and above 150°C, where the curve for bentonite is steeper. Natural Crook2 desorb less water than the corresponding nickel cation exchanged clay. It is interesting that nickel cations in bentonite have an opposite effect, according the TGA plot .

Figure 27 show how the derivatives from the plot in figure 26 varies with time. The derivative curves to the nickel exchanged clays support the almost identical TGA curve, and are overlapping for almost all temperatures. They both have a maximum mass loss rate when the sample temperature is 100°C. The fact that the mass loss rate at this point is slightly bigger in NiCrook2 than in NiBentonite help explain the difference in the total mass loss when the derivatives are identical for all other temperatures.
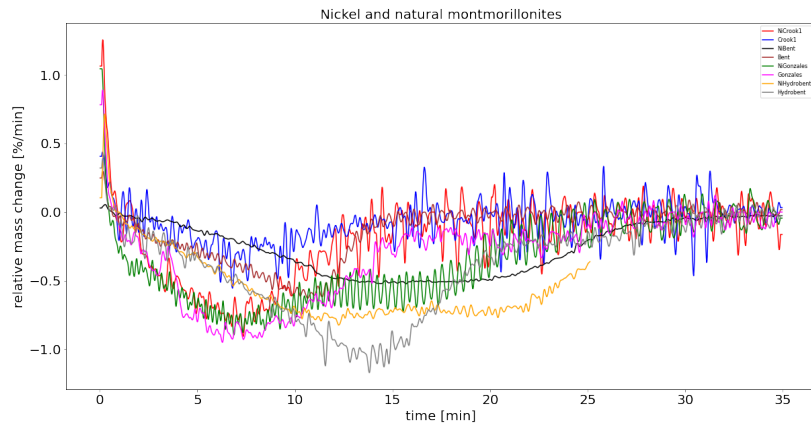
Figure 25: The thermogravimetric analysis plot of both natural and nickel cation exchanged clays shows how the relative mass change evolve when heating the samples according to TGA method 1 as illustrated in figure4.
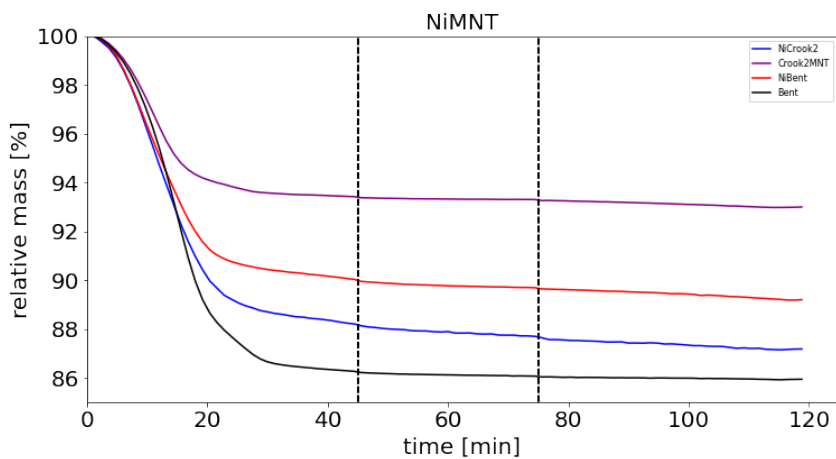
Figure 26: The thermogravimetric measurements for natural and nickel cation exchanged montmorillonites show how the relative mass change when heating the samples according to TGA method 2 as illustrated in figure5 with respect to time. The vertical dashed lines at 45 and 75 minutes show the time range when the sample was kept at 250°C.
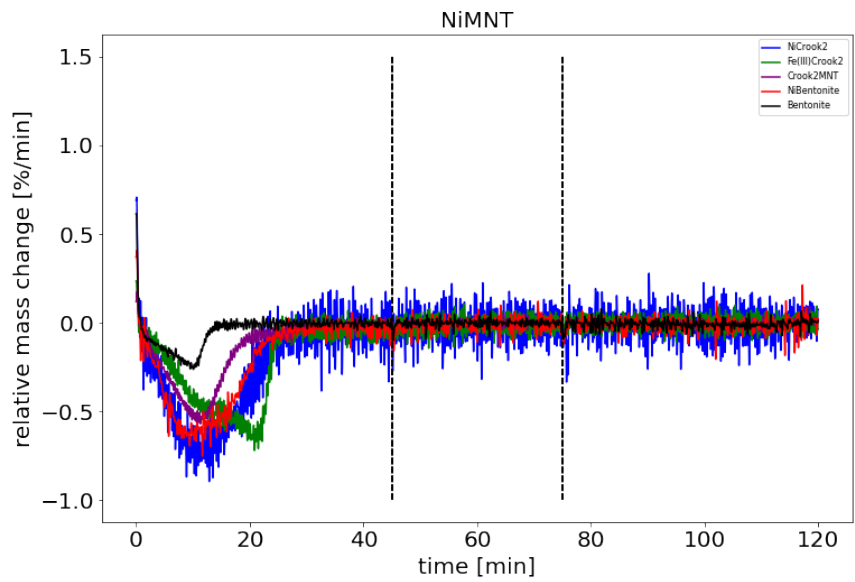
Figure 27: The plot show how the relative mass derivative in natural and nickel montmorillonite clays evolve with respect to time. The vertical dashed lines at 45 and 75 minutes show the time range when the sample was kept at 250°C.
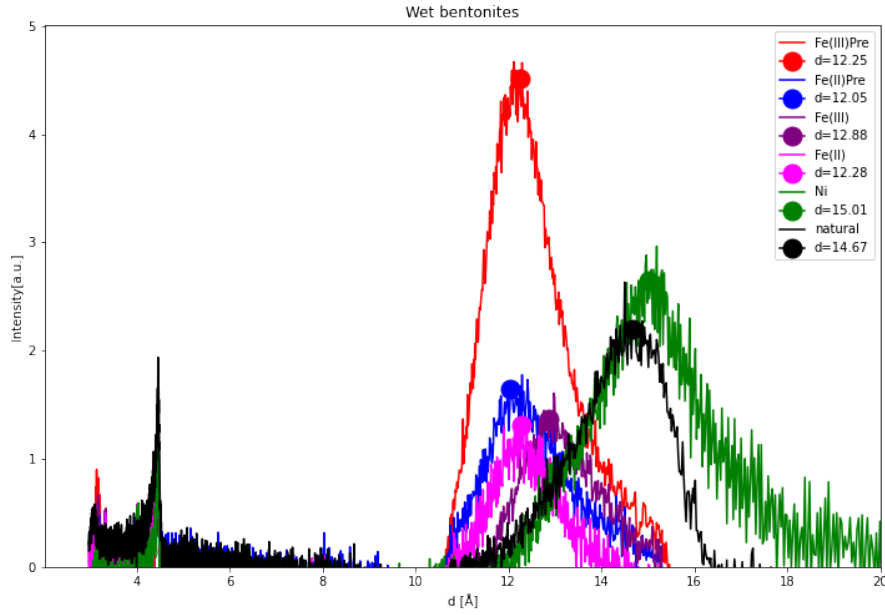
Figure 28: The x-ray diffraction patterns of the wet bentonites measured at the D8 instrument are illustrated. The d-spacings are plotted for each sample in the graph.

6.2 Iron bentonites

According to the first ESRF measurement series, is bentonite the clay that showed the best adsorption capacity of carbon dioxide and water. Therefore was some samples of bentonite clay, originating from the same reservoir as the bentonite clay that was cation exchanged with nickel, exchanged with iron(III) and (II) cations.

6.2.1 Powder x-ray diffraction

The raw x-ray diffraction patterns from D8 Focus are one dimensional, and plotted as a function of the basal distance d in Angstrom. The x-ray diffraction patterns of wet bentonites as measured with the D8 Focus diffractometer are presented in figure 28. The diffracted intensity of the dry bentonites have too low signal. This is a consequence of too low energy and too little x-ray flux in the scattering experiment. It is therefore necessary to measure them in a setup where this can be optimized, for instance in a setup similar to ESRF.

Among the wet clays, Fe(III)Pre bentonite has the sharpest signal at the first order Bragg peak, while nickel bentonite has the highest basal distance of 15.01 Å. The basal distance in the other clays, with their corresponding label from the x-ray diffraction patterns are listed in table 6. The letters "pre" indicate the bentonites swelled in water for 24 hours prior to the cationic exchange process.

Table 6: The d-spacings of wet and dry bentonites as measured with the D8 Focus diffractometer are listed accordingly in table as how they were prepared.

| Sample	d_{wet}[Å]
Fe(II) Pre	12.06
Fe(III) Pre	12.25
Fe(II)	12.28
Fe(III)	12.88
Ni(II)	15.01
Natural	14.67
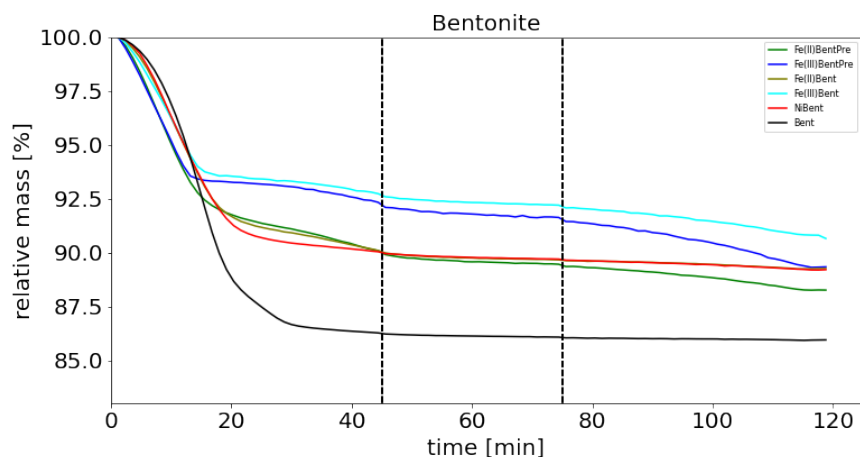
Figure 29: The thermogravimetric measurements for natural, nickel- and iron(II/III) cation exchanged bentonite show how the relative mass change when heating the samples on a ramp 5°C/min from 25°C to 250°C with respect to time. The letters "pre" indicate that the sample was swelled in water before cationic exchanged. The vertical dashed lines at 45 and 75 minutes show the time range when the sample was kept at 250°C.
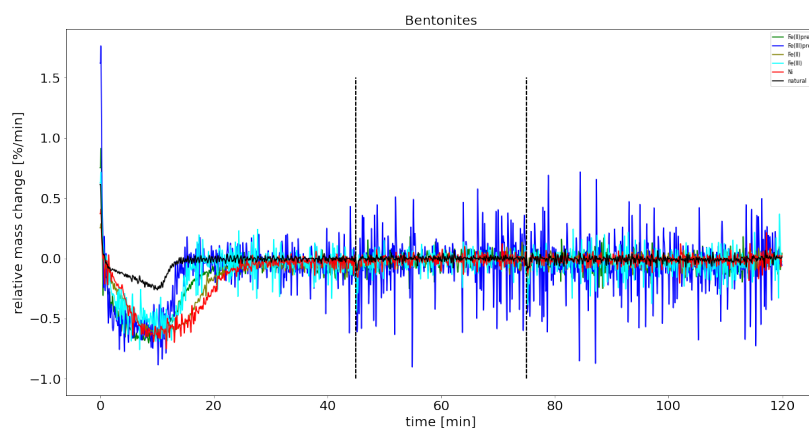
Figure 30: The plot show how the relative mass derivative in different bentonite clays evolve with respect to time. The letters "pre" indicate that the sample was swelled in water before cation exchanged. The vertical dashed lines at 45 and 75 minutes show the time range when the sample was kept at 250°C.

6.2.2 Thermogravimetric analysis

Figure 29 show how the relative mass in bentonites from the thermogravimetric measurement changes along the time frame specified in figure 5. It appears to be no significant difference in relative mass loss between the pre swelled clays and the ones without. Nickel and iron(II) bentonites have overlapping curves and loses around 10% of the initial mass during the entire measurement. Meanwhile, natural bentonite loses 13% while iron(III) exchanged bentonite loses 7.5%.

Figure 30 show how the derivatives of the TGA-plots in 29 varies in the same time frame. It becomes clearer to see that the mass loss is much slower in natural bentonite than in the cation exchanged samples. The derivatives also show that the mass loss in pre swelled iron(III)bentonite is slower compared with the simpler iron(III)bentonite while the sample temperature is below 100°C. The same tendency can be drawn from the derivative plots of the iron(II)bentonites. The mass loss rate on pre swelled iron(II)bentonite is scaled by $\frac{1}{2}$ compared with the other iron(II)bentonite.

7 Discussion

7.1 Nickel montmorillonites and bentonites

The general role of nickel cations in montmorillonite clays is an increasing layering distance, which was expected based on the results on fluorohectorites. The swelling results in an increase in the adsorption capacity of carbon dioxide and water molecules in the clay. This is most prominent in Crook2, according to the x-ray diffraction patterns gathered from the second ESRF measurements. The basal distance is bigger if there are either water molecules, carbon dioxide molecules or exchangeable cations in the interlayer. It is interesting that the final relative mass in the two thermogravimetric measurement series of natural bentonite differ with almost 10%. This can be explained by the random interstratification of bentonite. However, both of the TGA curves of nickel exchanged bentonite show that the cation exchanged clay is dry at 150°C, and desorb the same relative mass of water. The different results from the two ESRF measurements of nickel bentonite can be explained by that the clay measured in the first sequence was not completely dry. From the second measurement, we can draw a conclusion that nickel bentonite does not take up CO_2. Nickel Crook2 is more promising among the two clays that were set to dry for 3 hours. NiCrook2 has the largest layer spacing when it is dry, d= 10.36 Å, while the basal distance in NiBentonite is 10.13 Å. NiCrook2 is also the clay that swelled the most when exposed to CO_2. Compared with previous results on CO_2 intercalation in nickel fluorohectorite and Sodium Montmorillonite SWy-2, the NiCrook2 layers expand by 2 Å, which is double the swelled distance of pressurized nickel fluorohectorite and Sodium montmorillonite SWy-2[4].

Natural Crook2 montmorillonite with sodium cations in the interlayer, has a d-spacing almost 1 Å smaller than the Sodium montmorillonite SWy-2. Since the average d-spacing in Crook2 montmorillonite is below 10 Å, it was concluded not to take up CO_2, unlike sodium montmorillonite SWy-2. An explanation for the big basal distance difference may come from chemical differences in the source rocks, since they must have originated from different reservoirs.

The expected swelling from exchanging nickel cations with sodium, according to the experimental results with fluorohectorites, is 1.8 Å. While NaFluorohectorite did not take up CO_2, NiFlurohectorite swell with 0.9 Å as 40 bar of carbon dioxide is applied through the setup[7]. A similar tendency is observed in Crook2. The d-spacing in natural Crook2 with sodium cations is similar, but the increase is smaller in the montmorillonite that have been cation exchanged with nickel. This can be explained by that not all of the layers have been cation exchanged, giving a bigger lattice spacing disorder than NiFluorohectorite. However, the bigger increase in d-spacing for pressurized NiCrook2 suggest that this is a competitive material to its synthetic reference.

7.1.1 Powder x-ray diffraction

The expected step wise breakdown of two water layers when heating NiCrook2 is a good indication that this clay was completely dry. The initial diffraction pattern of NiCrook2 shows a d-spacing of 15.09 Å, and the total basal distance difference during the heating phase is almost 5 Å and 2WL. The aligning diffraction patterns obtained from cooling the sample is also a good pointer to this. The narrow Bragg peak at 0 bar suggest that most of the clay layers have the same thickness and have been cation exchanged with nickel. The double Bragg peak in pressurized NiCrook2 indicate that it takes up CO_2. The fact that the peak with lowest q has slightly higher intensity indicate that slightly more than half of the layers swell as the clay interact with 40 bar CO_2. The peak with the highest q-value align with the Bragg peak from the dry measurement, while the second peak correspond to a 2 Å increase of the interlayer. The broadening of the first order Bragg peak for increasing temperatures is also partly a consequence of increased particle interaction within the sample due to increased entropy. This change is very small as expected, since the temperature increase is relatively small. The fact that the basal distance difference between the double peaks is almost 1WL indicate that intercalation of CO_2 in Crook2 reminds of the water intercalation. The aligning diffraction patterns for vacuum pumped NiCrook2 before and after the CO_2 interaction indicate that all of the carbon dioxide molecules have been removed from the sample after vacuum was pumped into the CO_2-exposed NiCrook2. This is clearer in the pressure hysteresis plot of the d-spacing, showing that both of the NiCrook2 d-spacings measured at 0 bar are the same. Because of the bigger changes in the Bragg peak shape, Crook2 is the better candidate in comparison to the other

montmorillonites.

The x-ray diffraction pattern from the first ESRF measurement of the heated NiBentonite show a decrease in q_{001} compared with natural bentonite. The same tendency was also observed in the experiments with nickel fluorohectorites compared with sodium fluorohectorites[7]. The basal distance increases from 9.67 to 10.26 Å due to the cation exchange of nickel in bentonite. This improves the adsorption capacity considerably, since clays with a d-spacing lower than 10 Å do not adsorb CO_2 at all. The increase in q_{001} in the heated powder illustrate a decreasing water layer due to desorption of water. Also, since the peak position does not change after the temperature has been reduced to 27ºC, the powder can be assumed dry. The basal distance increase with increasing pressure as expected. The position of the shoulder at the first order Bragg peak when exposed to 50 bar align almost with the Bragg peak from the scan of the wet powder. This is a good indication for the NiBentonite clay to have been completely dry after it was heated for 2 hours. The shoulder itself suggest that the powder most likely was still wet, since it align well with the first order Bragg peak of the wet sample. Also, the fact that the basal distance in heated NiBentonite in the second ESRF measurement is slightly smaller than in the first measurement is a good pointer that this clay was not completely dry at the end of the heating phase.

It is an interesting feature concerning intercalation of CO_2 in nickel bentonite that the first order Bragg peak split into a double peak with the same maximum intensity when 50 bar CO_2 is applied. The peak with the lowest q-value align well with the Bragg peak from the measurement of wet nickel bentonite. The corresponding d-spacing of the second peak increase step wise with the pressure increase by in total 0.2 Å in response to carbon dioxide interaction. This indicate that almost half of the sheets adsorb very little carbon dioxide, while the rest interact with water molecules. The second half of the layers may also have interacted with carbon dioxide in a similar way as they would do with water molecules. However, it is more likely that this clay swelled in response to water molecules between the layers, since the measured basal distance in the nickel bentonite from the first experiment is higher than the second.

Among the measured clays in the first series of ESRF measurements nickel bentonite is the most promising to take up CO_2. The diffraction patterns for the wet, dry and pressurized sample are only almost overlapping with each other. The high lattice spacing disorder in bentonite gives an indistinct interlayer spacing for wet samples, and it is not clear how well the shoulder peak for pressurized clay align with the wet peak. The results from the second measurement series conclude that nickel bentonites does not adsorb CO_2.

In the second ESRF measurement series, nickel bentonite was dry before applying carbon dioxide into the capillary tube holding the clay. The plot of the time-dependent d-spacing in NiBentonite show that the d-spacing remain unchanged for the last minutes of the drying phase, even though it does not show a clear breakdown of two water layers compared with NiFlurohectorite and NiCrook2. However, with an initial basal distance measured at 14.31 Å, the total basal distance difference is almost 2WL, with a final average d-spacing of 10.13 Å. This indicate that NiBentonite also has been dried, and the thickness is smaller than it was measured in the first ESRF sequence. The change in basal distance for pressurized NiBentonite is very small, 0.02 Å, as presented in the pressure dependent plot in figure 13. The increase in d-spacing come from the increased lattice spacing disorder, which is illustrated by the broadening of the Bragg peaks. The broad peaks indicates that NiBentonite has a bigger lattice spacing disorder compared to both NiCrook2 and NiFluorohectorite. The alignment of the normalized Bragg peaks with the same peak position for dried and pressurized NiBentonite imply that there is no structural change when the clay is exposed to CO_2.

The distinct swelling in nickel hydrobentonite indicate there is some interaction between the clay and carbon dioxide at 36 bar. The scattered intensity is very low for the heated and pressurized sample, and the peaks are very broad. This correspond to high lattice spacing disorder. In terms of the average d-spacing, exchanged nickel cations contribute to a 0.5 Å swelling in hydrobentonite. When exposed to 41 bar carbon dioxide, NiHydrobentonite swell an additional 0.5 Å. However, when the pressure is further increased to 48 bar decreases the d-spacing back by 0.3 Å. This is an unusual effect in clays for increasing pressure compared with other experimental results, both on montmorillonites and fluorohectorites. However, considering the wide Bragg peaks the d-spacing in dry and pressurized nickel hydrobentonite is poorly defined, and the decrease may not be a fact at all. It would be interesting to collect new measurements on drying nickel hydrobentonite over a longer time period and with a bigger x-ray beam, to see if the same disorder is still valid.

During the cation exchange process with nickel in montmorillonites, Gonzales was considered the most promising sample. However, with a big drop in intensity and peak broadening, the d-spacing is poorly defined for this semi-dried powder. Gonzales was only measured at 41 bar and while drying it since the signal did not seem to change much during the measurement. Considering short drying time with a small change in peak position, the NiGonzales clay was still wet just before it was exposed to carbon dioxide. The change in peak width and height for the first order Bragg peaks in the x-ray diffraction pattern for Gonzales montmorillonite in response to drying and CO_2 interaction is caused by adsorption of water. The peak width and height decrease when the clay is drying, and increase when exposed to CO_2. The fact that the diffraction patterns for wet and pressurized Gonzales montmorillonite align confirm that the NiGonzales is not dry. The change in relative intensities at the higher order Bragg peaks, normalized with the maximum intensity of the first order Bragg peak, when varying temperature and pressure indicate that either water or CO_2 have been adsorbed in the clay. The similar form and position of the Bragg peaks between wet and pressurized CO_2 suggest that it is not completely dry at its driest. In this case, water has been adsorbed in the clay, rather than CO_2. The intensity for the first order Bragg peak decreased significantly after the first thirty minutes of drying. The sample was therefore assumed dry after a few minutes since there was no more change in peak width and position. The peak intensity increase when the powder was exposed to 41 bar of CO_2. Comparing the higher order Bragg peaks can sometime be useful, because smaller changes to the structure become more distinct in the higher order Bragg peaks. For instance is the Bragg peak position difference scaled by diffraction order n. The change in relative intensity and peak widths at the higher order peaks differ more than at the first order peak. The peaks for the wet powder is sharper than the peak for the pressurized powder, meaning that the maximum intensity is bigger and the peak is more narrow. The Bragg peaks in the diffraction pattern for the driest Gonzales powder are the broadest. As the temperature in the powder increases, the motion of the grains within the sample container increases. This result in broader peaks for dry Gonzales. Because the higher order peaks of the wet and pressurized Gonzales powder do not overlap each other, some of the CO_2 might have been adsorbed by the clay. The broadening of the dried Gonzales Bragg peaks come primarily from lattice spacing disorder.

The montmorillonite Crook1 seem to take up some CO_2. The diffraction patterns of dried and pressurized powder align well with similar intensities for the same q-values. The peak widths vary slightly more. The broadening of the Bragg peaks for the heated clay indicate that some of the layers swell more than others. A further peak broadening in response to pressure and the bigger peak shift at 50 bar is an interesting feature to NiCrook1. This indicate that not all of the layers swell in response to carbon dioxide, and that this occur only for high pressure. The peak shift at 50 bar correspond to swelling distance of 0.1 Å. The swelling of the interlayer in NiCrook1 montmorillonite and broadening of the first order Bragg peak at 50 bar CO_2 indicate that there are changes in the unit cell in the higher pressure regime. As there is hardly any changes in the d-spacing at 20 and 40 bar, the adsorption of CO_2 in NiCrook1 can be considered to be very slow. The basal distance difference is also much smaller than in NiCrook2. In other words, NiCrook2 is a better choice for CO_2 capture than NiCrook1. The basal distance is not as big compared with Crook2 either. However, we can be certain that nickel Crook1 take up CO_2 as well. The fact that the peak shift only happens at 50 bar indicate either that the reaction is very slow, or that the adsorption capacity is not very big. It is therefore expedient to study the carbon dioxide reaction for the same 52 minutes as the measurement of CO_2 intercalation in NiCrook2.

7.1.2 Thermogravimetric analysis

Nickel exchanged bentonite seem to be almost dry at 150°C, according to the results from the thermogravimetric measurements. This also yield for natural sodium bentonite. The ESRF measured d-spacing for both of the heated clays are therefore precise estimates for the basal spacing. The increased water intercalation indicate that there is more room for CO_2 in nickel bentonite than in sodium bentonite. Therefore, it seems like nickel cations improve CO_2 adsorption in bentonites, assuming that carbon dioxide intercalate similarly as water. Crook1 cation exchanged with nickel has been successfully dried at ESRF, according to the TGA measurements. There is no major mass loss after the sample temperature has reached 150°C, meaning that no more water evaporate from the interlayer at higher temperature. It is therefore very likely that the montmorillonite NiCrook1 adsorb some CO_2. NiCrook2 appear to be as good as dry at 150°C, according to the TGA and derivative plot. The thermogravimetric analysis of drying hydrobentonite indicate that the powder was not completely dry after heating it to 150°C at ESRF. It is therefore very unlikely that hydrobentonite is as promising as suggested from the ESRF ex-

perimental results. Gonzales was the other clay that do not seem to be dry at 150°C, confirming that the 30 minutes of heating the sample at ESRF was not enough to dry the clay completely. Because pumped vacuum was applied on the drying clays to help remove water molecules from the decreasing water layer in the ESRF setup, the clays may have been drier than the clays in the TGA measurement at 150°C. In other words, NiBentonite from the second ESRF measurement, NiCrook1 and 2 were all dry before the experiments with CO_2 began.

7.2 Iron bentonites

Iron seem to be a competitive cation to be exchanged with either sodium or calcium in fluorohectorites, as an alternative to nickel cations. It is therefore interesting to consider CO_2 adsorption in iron mont-morillonites, since iron is safer concerning health and environmental issues. Considering the TGA data, there is little difference in the pre-swelling and simpler preparation of the iron bentonites. The simpler prepared iron bentonites have a higher basal distance, according to the x-ray data obtained from the D8 Focus instrument. Because of this, the simple cation exchange preparation will be preferred. The fact that iron is slightly more abundant than nickel, is another motivation for studying iron cation exchanged montmorillonites[9]. However, considering the x-ray data on wet iron and nickel bentonites from the D8 Focus setup, together with the new ESRF data on nickel bentonite, it is not very promising that any of the iron bentonites take up CO_2.

7.2.1 Powder x-ray diffraction

The fact that the d-spacing in iron bentonites is smaller than the original sodium bentonite, result in a decreasing interest of iron cations as a substitute to nickel. The measured basal spacing of the wet iron bentonites lies between 12 and 13 Å, while it was measured to be 15.01 Å in wet nickel bentonite and 14.67 Å in natural bentonite with the same instrument. While it might seem that nickel bentonite is the better CCS candidate because of a higher d-spacing, the first ESRF measurement of wet nickel bentonite showed a basal spacing 12.5 Å, which is lower than wet Fe(III)bentonite, and more comparable with a 1WL interlayer structure. The second ESRF experiment series measured a d-spacing of 14.31 Å in wet NiBentonite, which is in a better agreement with the D8 Focus measurements. Since the layer spacing in wet iron bentonites are less than 14 Å, it is very likely that the basal distance in dry iron bentonites is lower than the 10.36 Å in nickel bentonite and 9.67 Å in natural bentonite. Heated iron bentonites with an expected layer spacing decrease of 2WL will have a d-spacing below 10 Å. It is therefore very unlikely that iron bentonites will take up CO_2.

The pre swelled Fe(III)bentonite had the highest intensity signal. For this reason, this clay is considered an interesting sample. The sharp first order Bragg peak from the x-ray diffraction pattern of pre swelled Fe(III)bentonite gives a precise estimate of the layer spacing. While the basal spacing is higher for the iron bentonites that were not swelled in water, the broader peaks correspond to higher random interstratification. Fe(III)Bentonite would be the most promising among the iron bentonites to take up carbon dioxide, since it has the highest basal spacing among the wet iron bentonites.

7.2.2 Thermogravimetric analysis

It is important to note that the iron bentonites requires higher temperature than nickel bentonite to be completely dry. It is also interesting that the iron(III) bentonite desorb less water than the other bentonites. The thermogravimetric analysis plot show that the mass change in iron bentonites is not flat, even at 200°C. On the other hand, the derivative plots show that the mass loss rate is close to zero after the temperature has reached 150°C. The mass loss rate is the same for all pre swelled iron bentonites below 125°C, and is similar to nickel- and natural bentonite. A similar comparison can be made between the two other iron bentonites, with mass loss rate slightly higher than in the pre swelled samples. Above 125°C, the mass loss rates appear to be more dependent of the charge than the type of atom. The TGA curve of the iron(III) bentonites flat out at lower temperatures than the other clays. This is partly because it has the least total relative mass loss. The curves of the iron(II) bentonites are not as flat, and the mass loss rates are net zero in the derivative plots. The aligning TGA curves for iron(II) bentonite and nickel bentonite suggest that they dry similarly.

It is necessary to dry the iron bentonites for more than 2 hours at 150°C when using a x-ray diffraction setup similar to the one at the Swiss-Norwegian beamline at ESRF, since the crystal structure of bentonites in general is destroyed at very high temperature. The nickel Crook2 montmorillonite and bentonite, which were heated for 3 hours appeared to be completely dry when using this heating procedure. The same drying time may apply for Fe(II)Bentonite, since they had a similar TGA curve. Iron(III)Bentonite dries more easily than the other bentonites, so the clay powder should be completely dry after it has been heated for 3 hours in the ESRF setup as well. However, the iron bentonites are expected not to take up CO_2. Therefore should other, more promising samples be prioritized before them. This could be the montmorillonites Crook1, Crook2 and SWy-2, exchanged with the most effective cations as tested on fluorohectorites.

8   Conclusion

Among all of the natural smectites that have been studied, nickel Crook2 is the most promising to take up carbon dioxide, and it is therefore also the best candidate as material for carbon capture. As expected, carbon dioxide behaves similarly to water in this clay. The higher the basal distance is in a dry clay mineral, the more distinct the swelling is in response to carbon dioxide. Nickel bentonite is the other clay that was properly measured dry and when exposed to CO_2, but these measurements prove that it does not take up carbon dioxide for pressures below 40 bar. This is unexpected, considering that bentonite clays are known to adsorb more water compared to other montmorillonites. The x-ray diffraction measurements from ESRF show that nickel montmorillonite Crook1 swell if the CO_2 pressure is above 40 bar. Just like in fluorohectorites, the cation exchange with nickel causes the interlayer in montmorillonites to swell more compared to the clay interlayers with either sodium or calcium cations. From the thermogravimetric measurements of water intercalated clays, nickel bentonite, nickel Crook1 and nickel Crook2 montmorillonites were the clays that dried the fastest and desorbed the least water. The results confirm that they are dry after they have been heated at 150°C for 3 hours. For this reason, the increasing layer thickness of the pressurized montmorillonites is an effect that they take up carbon dioxide, and not water. There is a clear trend that the lattice spacing disorder in clays increases with increasing temperature.

For further studies, it is interesting to study the structural change in NiCrook2 at smaller pressure steps of CO_2, in order to determine the minimum threshold that is required before the clay intercalates with CO_2. This can further help determine how efficient carbon adsorber NiCrook2 may be. Another important approach is to determine the quantity of adsorbed CO_2 in NiCrook2 at different pressure and temperature through adsorption measurements with an IsoSORP gravimetric sorption analyzer. It may also be interesting to measure properly iron bentonites, intercalating with CO_2 before any final conclusion on them can be made. Nickel Gonzales and hydrobentonite could also be remeasured with increased beam size and energy of the x-ray photons, since the expected higher intensity will give a better estimate on the d-spacing as it dries. It could be interesting to see if higher pressure of carbon dioxide would result in a 2WL swell in NiCrook2. Another interesting study would be to look at the CO_2 adsorption in cation exchanged Ni- and Fe(III) montmorillonite SWy-2 clay, since the sodium montmorillonite SWy-2 take up CO_2.

References

[1] Y. Chen and D. Lu. 'CO2 capture by kaolinite and its adsorption mechanism'. In: *Applied Clay Science* 104 (2015), pp. 221–228.

[2] J. Dehn and S.R. McNutt. *The Encyclopedia of Volcanoes (Second Edition)*. 2015, pp. 1285–1294.

[3] V. Dyadkin et al. 'A new multipurpose diffractometer PILATUS@SNBL'. In: *J. Synchrotron Rad.* 23 (2016), pp. 825–829.

[4] P. Giesting et al. 'Interaction of carbon dioxide with Na-exchanged montmorillonite at pressures to 640 bars: Implications for CO2 sequestration'. In: *International journal of greenhouse control* 8 (2012), pp. 73–81.

[5] Hilgenberg. *MARK-TUBES MADE OF BOROSILICATE GLASS*. URL: https://www.hilgenberg-gmbh.de/en/catalog/test-tubes/mark-tubes/detail/?tt_products5BbackPID5D=158&tt_products5Bproduct5D=32&cHash=.

[6] K.W.B. Hunvik et al. 'CO_2 Absorption Enhanced by Tuning the Layer Charge in a Clay Mineral'. In: *Langmuir 2021* 37 (2021), pp. 14491–14499.

[7] K.W.B. Hunvik et al. 'Intercalation of CO2 Selected by Type of Interlayer Cation in Dried Synthetic Hectorite'. In: *Langmuir* 39 (2023), pp. 4895–4903.

[8] P. Loch et al. 'Spontaneous formation of an ordered interstratification upon Ni-exchange of Na-fluorohectorite'. In: *Applied Clay Science* 198 (2020).

[9] *Metaller*. URL: https://www.fhi.no/nettpub/luftkvalitet/temakapitler/metaller---luftkvalitetskriterier/.

[10] J. M. Moreno-Maroto and J. Alonso-Azcárate. 'What is clay? A new definition of "clay" based on plasticity and its impact on the most widespread soil classification systems'. In: *Applied Clay Science* 161 (2018), pp. 57–63.

[11] H. Kodama R. E. Grim. *clay mineral*. URL: https://www.britannica.com/science/clay-mineral.

[12] Vyacheslav Romanov. *Greenhouse gases and clay minerals*. 2018.

[13] P.M. Røren et al. 'Controlled sample environment for studying solid-gas interactions by in situ powder X-ray diffraction'. In: *Journal of applied crystallography* (2020).

[14] da Silvam G.J. et al. 'Synchrotron x-ray scattering studies of water intercalation in a layered synthetic silicate'. In: *Physical review E* 66 (2002), p. 011303.

[15] X. Wang, Y. Li and H. Wang. 'Structural Characterization of Octahedral Sheet in Dioctahedral Smectites by Thermal Analysis'. In: *Minerals* 10 (2020).

[16] M.S. Yılmaz, Y. Kalpaklı and S. Pişkin. 'Thermal behavior and dehydroxylation kinetics of naturally occurring sepiolite and bentonite'. In: *Journal of Thermal Analysis and Calorimetry* 114 (2013).